Studies on the anticancer effect of bisabosqual A, as a novel asparagine synthetase inhibitor, in human non-small cell lung cancer cells

2023

Yanjun Pan

Content

Preface

Asparagine synthetase (ASNS), an imperative enzyme for the *de novo* biosynthesis of asparagine (Asn), becomes a promising anticancer target. In several solid tumors, ASNS expression exhibited positive correlation with tumor growth, including lung cancer, breast cancer and gastric cancer. Moreover, overexpressed ASNS was associated to the chemoresistance and metastasis *in vivo*, while ASNS knockdown constrained tumor growth in mouse xenograft models. Asn depletion was considered a vital factor in anticancer effect after ASNS knockdown. Cancer cells demand for abundant nutrition to support their rapid proliferation, and thus amino acid depletion, such as Asn or glutamine (Gln) depletion, is a prospective strategy for inhibiting cancer through the impact on metabolic vulnerability. Therefore, ASNS inhibition becomes a potential cancer chemotherapy.

No ASNS inhibitors have been used clinically so far. Most of ASNS inhibitors are the analogs of β-aspartyl-AMP intermediate or transition-state in ASNS reaction. Although transition-state analogs could suppress ASNS at nanomolar concentrations *in vitro*, their low cell permeability and instability obviously impeded their anticancer activity in cells. Consequently, it is urgent to develop ASNS inhibitors with a novel pharmacophore as well as effective anticancer activity. In this study, an *in vitro* screening system was established and applied in our *in-house* microbial metabolite library. Subsequently, a unique bisabolane-type meroterpenoid molecule bisabosqual A (Bis A), was identified as a hit molecule of ASNS inhibitor, and was found to be able to covalently modify K556 site of ASNS (Chapter 1). Our data, for the first time,

revealed the potential of K556 site on ASNS to affect the efficacy of ASNS inhibitors.

Higher ASNS expressions were observed in lung cancer tissues than in normal lung tissues, and the cell growth of non-small cell lung cancer (NSCLC) was impaired by ASNS knockdown. However, further study about anticancer effectiveness and underlying mechanism of ASNS inhibitors was scantily focused on. Accordingly, this study investigated the anticancer mechanism of Bis A in human NSCLC cells. In Chapter 2, Bis A was observed to exert anticancer activity through promoting oxidative stress and apoptosis, while impeding autophagy, cell migration and epithelial-mesenchymal transition (EMT), even though it activated negative feedback pathways, including GCN2-eIF2α-ATF4, PI3K-AKT-mTORC1 and RAF-MEK-ERK pathways. In addition, the synergistic effect of Bis A with L-ASNase or the mTOR inhibitor (rapamycin or torin-1), showed a prospective strategy for cancer chemotherapy.

Chapter 1 Identification of bisabosqual A as a potential ASNS inhibitor and investigation of the binding site of bisabosqual A on ASNS

1.1 Introduction

ASNS is mainly located in the cytoplasm, with function of catalyzing aspartate (Asp) and Gln to produce Asn and glutamate (Glu) [1]. Human ASNS (hASNS) contains two conserved domains, the N-terminal (residues 1-216) glutaminase domain as well as the C-terminal (residues 217-561) synthetase domain, and its high-resolution crystal structure was reported, although missing many residues from the structure, such as residues 536-561 in the C-terminal domain [2]. Its ATP-dependent catalytic reaction starts from the activation of an Asp carboxyl group in the C-terminal domain, followed by the formation of a β-aspartyl-AMP intermediate. The ammonia produced by the hydrolysis of Gln in the N-terminal domain is transferred through an internal ion channel, initiating a nucleophilic attack on the β-aspartyl-AMP intermediate to produce Asn in the C-terminal domain [3].

Asn, a non-essential amino acid, plays an important role in protein synthesis and rate limitation of translation [4]. Due to the importance of amino acid in cancer development, the depletion of some amino acids, including Gln, Asn, and cysteine, effectively inhibited cancers such as breast cancer, leukemia, and prostate cancer [5–7]. A classical case is that L-asparaginase (L-ASNase), an enzyme depleting Asn through hydrolysis, has been approved by the US Food and Drug Administration (FDA) to cure acute lymphoblastic leukemia (ALL) patients for decades [8]. ALL cells exhibit a

primary low ASNS level, preventing from producing Asn, and thus L-ASNase can be significantly effective in ALL patients, but drug resistance was observed in some ALL patients with an increase of ASNS expression [9, 10]. Moreover, ASNS level has a negative correlation with the efficacy of L-ASNase in some solid tumors, revealing the importance of ASNS expression in disrupting Asn deprivation to support cancer development [9]. Apart from that, the overexpression of ASNS was related to tumor growth [11], while ASNS knockdown was shown to hinder tumor growth in mouse xenograft models and a more significant inhibitory effect was found after combination of ASNS knockdown and L-ASNase [4, 12]. Therefore, ASNS is a potential molecular target for cancer chemotherapy.

There are currently no ASNS inhibitors clinically used, and chemo-types of ASNS inhibitors are limited, including analogs of Gln, Asp, β-aspartyl-AMP intermediate or transition-state and platinum (II) compounds [13–16]. Even though transition-state analogs suppressed hASNS at a nanomolar concentration *in vitro*, their low cell permeability and instability impaired their antiproliferative activities in L-ASNase-resistant leukemia MOLT-4 cells, with IC_{50} reaching up to 100 μM [15]. Consequently, it is urgent to develop ASNS inhibitors with a novel pharmacophore and effective anticancer activity.

The inorganic pyrophosphate (PP_i) production indicating the formation of β-aspartyl-AMP intermediate, was usually used to measure ASNS activities [14, 15, 17]. However, PP_i production could not reflect the complete of whole ASNS reaction containing the catalysis of N-terminus. Hence, a new *in vitro* screening system by using

purified recombinant hASNS needs to be constructed to evaluate the ASNS activity.

1.2 Material and Methods

1.2.1 Chemicals

Bisabosquals A and B were isolated from culture broths of the fungi *Stachybotrys* sp. RF-7260, and Bisabosquals C and D were isolated from culture broths of the fungi *Stachybotrys ruwenzoriensis* RF-6853 [18]. The purity of bisabosqual derivatives is >99% in the HPLC analysis.

1.2.2 Expression and purification of recombinant hASNS

In accordance with Bac-to-Bac Baculovirus Expression System manual (Invitrogen), the expression and purification of recombinant hASNS was conducted. The recombinant bacmid DNA was obtained, through *E. coli* DH10Bac being transformed with the plasmid pDEST8 containing cDNA of hASNS with a GST tag at the N-terminus or a 6×His tag at the C-terminus, and subsequently, was transfected into *sf9* insect cells to produce recombinant baculovirus. The recombinant hASNS was extracted from *sf9* cells infected with ASNS-expressing baculovirus (MOI = ~1.0), and then was purified using a Ni^{2+}-NTA column. *Sf9* cells were cultured in Sf-900 III SFM medium (Gibco) at 28°C. The wild type (WT) and K556A mutant of ASNS without tag were obtained after using Turbo3C Protease (Accelagen) to cleave GST-ASNS.

1.2.3 ASNS activity measurement

2.2 μg of recombinant hASNS was treated with compounds in 50 μL of mixture containing 10 mM L-Gln, 10 mM L-Asp, 1 mM ATP, 5 mM $MgCl_2$, 1 mM DTT, and 20 mM Tris-HCl (pH 7.5), at 37°C for 30 min, followed by heating at 100°C for 10 min to stop reaction. Then, according to manufacturer′s instructions, AMP concentrations were detected by using AMP-Glo™ assay kit (Promega), to evaluate the ASNS activity.

1.2.4 PP_i measurement

PP_i measurement was performed based on a previous report [15]. In Brief, the mixture consisting of 10 mM L-Asp, 25 mM L-Gln, 10 mM $MgCl_2$, 0.5 mM ATP, 100 mM EPPS buffer (pH 8.0), pyrophosphate reagent (35 μL), and compound, was prepared. After adding 4 μg of recombinant hASNS into the mixture, the absorbance at 340 nm was detected for 10 min.

1.2.5 Thermal shift assay

1 μM recombinant hASNS was incubated with Bis A for 30 min at 37°C, followed by heating at 37, 42, 47, 52, 57, or 62 °C for 2.5 min. Then, the protein was centrifuged at 15,000 rpm for 30 min at 4 °C. The supernatants were subjected to the SDS-PAGE and stained with Coomassie Brilliant Blue (CBB).

1.2.6 LC-MS/MS analysis

After incubation of the recombinant hASNS and Bis A for 30 min at 37°C, samples were subjected to the SDS-PAGE and CBB staining. The protein bands of groups

treated with 0 μM and 3 μM Bis A were excised and digested with a trypsin in the gels. The digests were separated by using nano-LC (EASY-nLC 1000, Thermo Fisher Scientific) on a nano-capillary column (NTTC-360/75-3-105, Nikkyo Technos) following tandem mass spectrometry (Q Exactive mass spectrometer, Thermo Fisher Scientific) equipped with a nano electrospray ion source. MS and MS/MS spectra were acquired using the TOP 10 method in positive mode. The obtained data were analyzed with MASCOT (version 2.7.0, Matrix Science) and Proteome Discoverer (version 2.4, Thermo Fisher Scientific). A MASCOT search was carried out against the in-house database, including ASNS, using the following parameters: enzyme = trypsin; maximum missed cleavages = 3; variable modifications = acetyl (protein N-term), Gln- > pyro-Glu (N-term Q), oxidation (M), propionamide (C), Bis A (K: 366.18311 Da); product mass tolerance = ± 15 ppm; product mass tolerance = ± 30 milli mass units; and instrument type = ESI-TRAP. The MS chromatograms (Figure 3B) corresponding to the peptide “TLTHYKSAVK” and its Bis A-modified peptide were extracted at m/z = 574.3273 and m/z = 757.4193, respectively, with MS tolerance of ±15 ppm using Qual browser (version 4.1.31.9, Thermo Fisher Scientific). Similarly, the MS chromatograms were plotted with the following settings: “EILWRPKEAFS” m/z = 688.3713 and 871.4619 (Figure 3C). The modification rate (Figure 3A) was calculated as follows: (area of Bis A-modified peptide)/(area of Bis A-modified peptide + area of unmodified peptide) ×100. MS spectra of TLTHYKSAVK peptide and Bis A-modified TLTHYKSAVK peptide (Figure 3B) were created in Qual browser.

1.2.7 Covalent docking

The three-dimensional structure of ASNS (AF-P08243-F1-model_v3.pdb) downloaded from the AlphaFold Protein Structure Database [19–21] was used to perform the covalent docking simulation. Through using CovDock pose prediction mode and MM-GBSA scoring in Schrödinger, covalent docking simulation was executed [21– 23]. The pose with the highest rank was chosen for the covalent complex.

1.2.8 Statistical analysis

The data were presented as mean ± SEM values of three or more than three independent experiments and subjected to one-way ANOVA and Dunnett's multiple comparison tests by using the GraphPad Prism software. Statistical significance was determined at $P < 0.05$.

1.3 Results

1.3.1 Bis A is a potential ASNS inhibitor

For evaluating ASNS activities, an *in vitro* screening system was established to detect the concentration of AMP, a product in ASNS catalysis reaction (Figure 1A). After using this system to screen our *in-house* microbial metabolite library [24], Bis A was observed to significantly inhibit ASNS activity, with an IC_{50} of 10.7 μM (Figure 1B). Bis A is a unique bisabolane-type meroterpenoid molecule (Figure 1C), which is produced by the fungus *Stachybotrys* sp. RF-7260. In the structure-activity relationship (SAR) study, bisabosquals B, C, and D, the analogs of Bis A, also exhibited ASNS

inhibitory activities, but much lower than that of Bis A, confirming that Bis A was a hit molecule (Figure 1C and D). And the results suggested that their common skeleton was conducive to suppressing ASNS activity, and the two vicinal aldehyde groups at C3' and C4', hydroxyl group at C5, as well as the double bond between C10 and C11 in chemical structures had impact on their interaction with ASNS (Figure 1C and D). The PP_i level was measured to determine the ASNS activity in many studies, and thus this method was performed to further confirm whether Bis A was a potential ASNS inhibitor. The results showed that PP_i concentrations decreased after treatment with Bis A, in a dose-dependent manner (Figure 1E), revealing that Bis A hindered the formation of β-aspartyl-AMP intermediate to inhibit ASNS activity. Accordingly, Bis A was identified as a promising ASNS inhibitor.

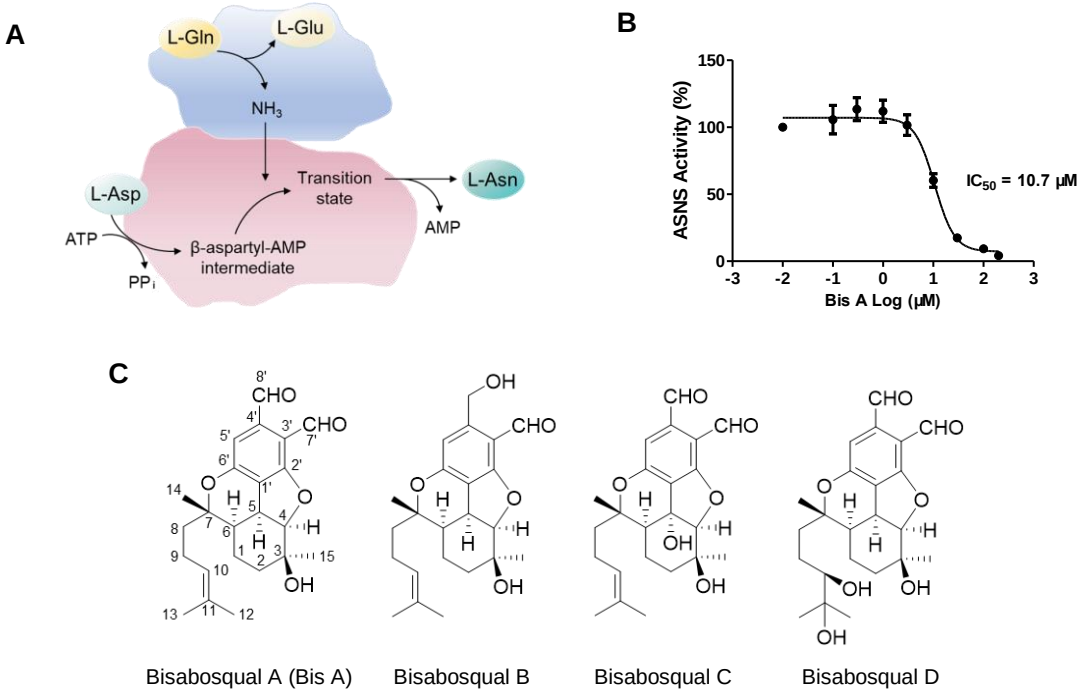

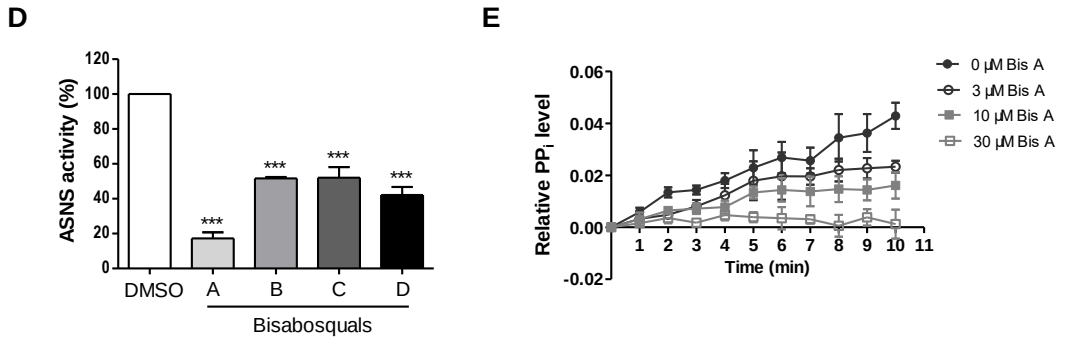

Figure 1. The effect of Bis A and its analogs on ASNS activity. (A) The catalysis of ASNS. The bule and red present the N-terminal glutaminase domain and C-terminal synthetase domain, respectively. (B) The activity of recombinant hASNS treated with Bis A (n = 5). (C) The chemical structures of Bis A as well as its analogs, bisabosquals B, C, and D. (D) The activity of ASNS after administration of Bis A or its analogs at 20 μM (n = 3). (E) Relative PP_i level generated in ASNS catalytic reaction (n = 3). Data are represented as mean ± SEM; P values were determined by one-way ANOVA with Dunnett's multiple comparisons test. ***$P < 0.001$.

1.3.2 Action mode of Bis A on ASNS

To investigate the action mode of Bis A on ASNS, ASNS was incubated with Bis A, and subsequently, was subjected to SDS-PAGE and CBB staining. As shown in Figure 2A, a dose-dependent intensity decreasing for the ASNS band was observed upon the application of increased concentration of Bis A, as well as the band shifting to a larger molecular weight. This result suggested that Bis A was possible to covalently bind ASNS and partially promote ASNS aggregation. In addition, their binding was further revealed, when Bis A increased ASNS stability exposed to a certain degree of heating (Figure 2B and C). Therefore, the binding site of Bis A on ASNS was considered to be studied.

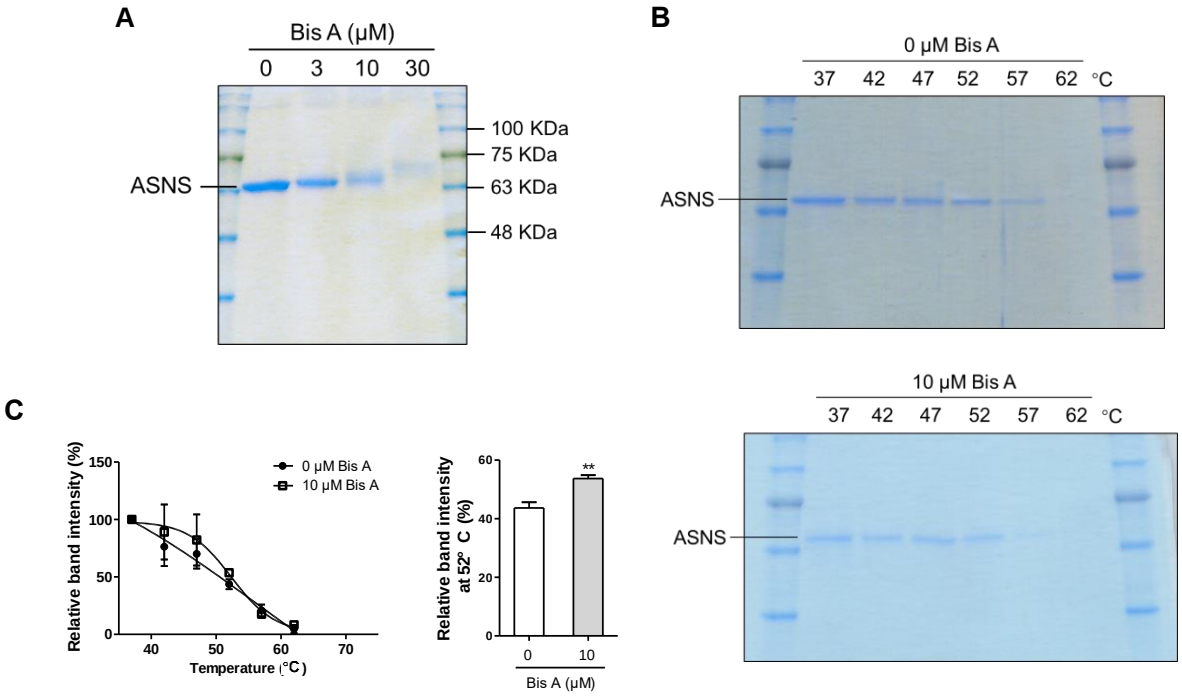

Figure 2. The potential of Bis A covalently binding ASNS. (A) The intensity of recombinant hASNS on an SDS-PAGE gel. (B) The intensity of ASNS after incubation with DMSO (upper) or Bis A (lower) and subsequently heating at different temperatures. (C) The quantification of (B). Relative band intensity (the percentage of T_X to T_{37}) at 37, 42, 47, 52, 57, 62°C (left) (n = 3), and 52°C (right) (n = 5).

1.3.3 Binding site of Bis A on ASNS

To explore the binding site of Bis A on ASNS, LC-MS/MS was used to analyze the stained band of groups administrated by 0 or 3 μM Bis A in Figure 2A. K467 and K556 sites of ASNS were identified to be modified by Bis A, further indicating the covalent binding between Bis A and ASNS (Figure 3A–C). Notably, the evidently higher modification rate of Bis A on K556 site (Figure 3A and B) disclosed that K556 site presumably was important to the ASNS inhibitory activity of Bis A. Furthermore, to validate the feasibility of the binding, AlphaFold2 model structure of ASNS was predicted. By using CovDock, a covalent docking simulation with the reactive receptor

residue K556 on the ASNS model structure was executed [22, 23]. As shown in Figure 3D, a ligand binding pocket near K556 was confirmed, as well as a covalent docking pose of the ASNS-Bis A complex (Figure 3E). The results suggested the covalent binding between the aldehyde group at C3' position of Bis A and K556 *via* Schiff-base formation. Next, K556A mutant that lysine was replaced by alanine at the 556 site of ASNS was constructed. Similar ASNS activities were observed in WT and K556A mutant, but ASNS inhibitory activity of Bis A could not be detected in K556A mutant (Figure 3F and G). Consequently, these results revealed that Bis A could exert ASNS inhibitory activity through binding the K556 site of ASNS.

A

Peptide	Modification rate (%)
EILWRPKEAFS K467-Bis A (366.18311 Da)	2.03
TLTHYKSAVK K556-Bis A (366.18311 Da)	15.93

B

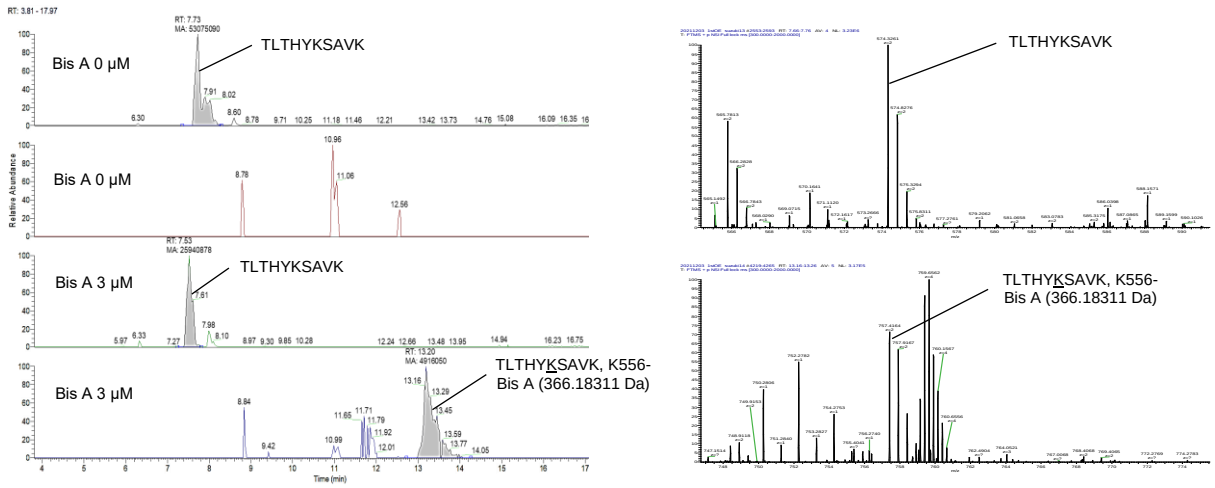

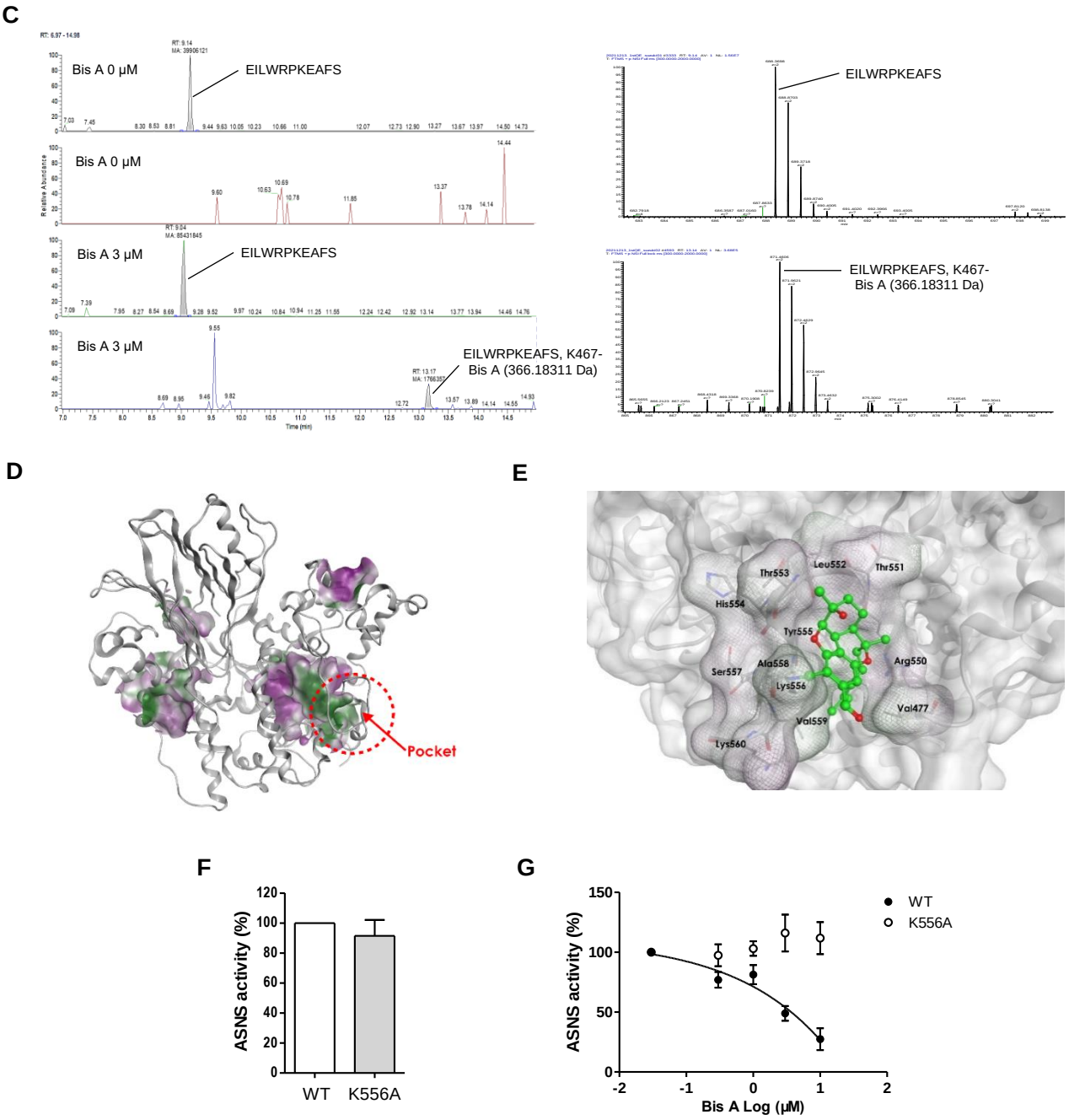

Figure 3. The binding sites of Bis A on recombinant hASNS. (A) The modification sites of Bis A on ASNS after LC-MS/MS analysis. In the analysis of the indicated peptide, the modification rate (%) represents the percentage of the abundance of the modified peptide in the total abundance of the corresponding peptide. (B,C) The LC-MS/MS results showing Bis A modified the K556 site (B), or the K467 site (C) on ASNS. (D) The molecular surface of ligand binding sites on the ribbon model of the hASNS structure from AlphaFold2. Hydrophilic, lipophilic, and neutral sites on the molecular surface was indicated by purple, green, and white, respectively. (E) The prediction of a covalent docking pose of ASNS-Bis A complex by CovDock. Carbon and oxygen atoms were representd by green and red balls, respectively. (F) The original ASNS activity of WT or K556A mutant. (G) ASNS activities of WT and K556A mutant exposed to Bis A (n = 3). Data are represented as mean ± SEM.

1.4 Discussion

The shortage of ASNS inhibitors restricts the deep insight of ASNS as an anticancer target, so there is an urgent need to develop novel ASNS inhibitors. In this study, a fungal metabolite, Bis A, containing a unique bisabolane-type meroterpenoid was identified as a new ASNS inhibitor. Bis A has a different pharmacophore from the ASNS inhibitors reported so far (Figure 1).

Bis A influenced the aggregation and stability of the recombinant hASNS (Figure 2). LC-MS/MS analysis and computational simulation indicated its aldehyde group could covalently modify K556 site in the C-terminal synthetase domain of ASNS (Figure 3). And a high likelihood binding pocket of Bis A near K556 site were observed in our AlphaFold2 model structure, even though X-ray structure of hASNS does not include K556 site [2]. Bis A did not show ASNS inhibitory activity in K556A mutant (Figure 3G), for the first time indicating the importance of K556 site in ASNS inhibition. Besides, our study showed Bis A could slightly modify K467 site in the C-terminal synthetase domain of ASNS, and obstruct the formation of β-aspartyl-AMP intermediate (Figure 1E, 3A, and 3C). The side chain of K467 was found to form an electrostatic interaction with the phosphate moiety of β-aspartyl-AMP intermediate in human ASNS [2], and as a conserved residue, K467 was vital for catalysis of AS-B (asparagine synthetase B in *Escherichia coli*) [25]. This implied that Bis A was probably to modify K467 site of ASNS to influence the electrostatic interaction between the active intermediate and ASNS to further inhibit ASNS activity.

The chemical structure of this new pharmacophore on Bis A, as well as the

information of the binding site, could provide strong support for further SAR studies and the development of ASNS inhibitors.

Chapter 2 Anticancer effect and mechanism of bisabosqual A in non-small cell lung cancer cells

2.1 Introduction

Lung cancer is one of the leading causes of cancer deaths worldwide, with non-small cell lung cancer (NSCLC) accounting for around 80% incidence of lung cancer [26]. Higher ASNS levels was expressed in lung cancer tissues and ASNS expression showed a negative correlation with survival of NSCLC patients, while knocking down ASNS promoted anticancer activity [27, 28]. Nonetheless, there is limited research regarding the anticancer efficacy and underlying mechanism of ASNS inhibitors in NSCLC. Consequently, NSCLC cells were used in this study to investigate the anticancer effect of Bis A.

Apart from the canonical function in protein synthesis, ASNS was involved in MAPK cascade activation, cellular stress response, and amino acid exchange [11]. ATF4 as a transcription regulator of ASNS, plays a vital role in ASNS expression, which participates in GCN2-eIF2α-ATF4 axis of amino acid response (AAR) pathway [29]. As the product of ASNS catalysis reaction, Asn was regarded as an amino acid exchange factor to influence the uptake of histidine, serine, and arginine, which could regulate mTORC1 activity and nucleotide synthesis [30]. Moreover, ASNS was reported to affect metastatic potential *in vivo*, which was correlated with the regulation of epithelial-to-mesenchymal transition (EMT) [31, 32]. Accordingly, these factors were considered in investigating the anticancer mechanism of Bis A.

Asn in the extracellular environment is deprived by L-ASNase, while the *de novo* biosynthesis of intracellular Asn is regulated by ASNS to promote drug resistance [9]. Considering the strategy of simultaneously reducing intracellular and extracellular Asn levels, it was necessary to study the anticancer effect of combination treatment of Bis A and L-ASNase.

2.2 Material and Methods

2.2.1 Chemicals

The following chemicals were purchased from the indicated sources: DL-α-tocopherol, chloroquine diphosphate (CQ), and TGF-β (Nacalai Tesque), L-asparagine monohydrate (Wako), torin-1 (LKT Laboratories), rapamycin (Enzo Life Sciences), Z-VAD-FMK (Peptide Institute), and TAK-475 and L-ASNase from *E. coli* (Sigma-Aldrich).

2.2.2 Cell culture

A549 cells (RIKEN Bioresource Research Center) were cultured in DMEM (12100-061, Gibco) supplemented with 10% FBS and H1299 cells (American Type Culture Collection) were cultured in RPMI 1640 (31800-089, Gibco) supplemented with 10% FBS, in a 5% CO_2 incubator at 37°C.

2.2.3 Cell viability

In 2D-culture, 0.5×10^4 A549 cells or 0.3×10^4 H1299 cells per well were seeded into

a 96-well flat bottom plate, and in 3D-spheroid, 0.25×10^4 A549 cells or 0.15×10^4 H1299 cells per well were seeded into a 96-well ultra-low attachment round bottom plate, and then cultured for 24 h [33], followed by administration of Bis A, with or without Asn or the indicated inhibitors. After 72 h of culture, a CCK-8 assay kit (Dojindo) was used to evaluate the cell viability. 0.5% or 1% DMSO was included in compound alone treatment or co-treatment. Unless indicated otherwise, the viability assay was conducted in 2D-culture.

2.2.4 siRNA transfection

One-step transfection was employed for siRNA transfection, and ScreenFect siRNA Transfection Reagent (Wako) or Lipofectamine RNAiMAX Transfection Reagent (Invitrogen) were used for siASNS or siFDFT1 transfection, respectively. The cell suspension (2×10^4 cells/well in a 24-well plate or 3×10^3 cells/well in a 96-well plate) was mixed with siRNA-lipid complex, followed by incubation for 48 h. Cells in a 96-well plate were exposed to compounds for 48 h or 72 h, and then were subjected to the CCK-8 assay kit to detect cell viability. Cells in a 24-well plate were collected to measure the expression of proteins. ON-TARGETplus Non-targeting siRNA #1, as well as ON-TARGETplus Human ASNS (440) siRNA - SMARTpool and ON-TARGETplus Human FDFT1 (2222) siRNA - SMARTpool were purchased from Dharmacon Reagents (Horizon Discovery). Sequences of siRNA are as follows: ON-TARGETplus Non-targeting siRNA #1 (UGGUUUACAUGUCGACUAA), ON-TARGETplus Human ASNS (440) siRNA - SMARTpool (GGGUAGAGAUACAUAUGGA,

UAUGUUGGAUGGUGUGUUU, GGUGAAAUCUACAACCAUA, and GUAAAGAAACGUUUGAUGA, and ON-TARGETplus Human FDFT1 (2222) siRNA - SMARTpool (GGAAGAGAUUUAUCAUAGA, GUGUUUAACUUCUGUGCUA, GUUUGGAGCAGGUAUGUUA, CAACGCAGUGUGCAUAUUU).

2.2.5 Cellular thermal shift assay

Referring to a previous report [34], the cellular thermal shift assay (CETSA) was performed. After incubation of the cell lysate and Bis A for 30 min at room temperature, samples were heated at 37, 47, 52, 57, 62, 67, or 72 °C for 5 min and then centrifuged at 15,000 rpm for 30 min at 4 °C. The supernatants were collected for conducting western blot assay.

2.2.6 Western blot assay

Cells were lysed by 0.5% Triton X-100 with protease inhibitor cocktail (Nacalai Tesque) and phosphatase inhibitor cocktail (Nacalai Tesque) in PBS. Protein samples were subjected to SDS-PAGE and transferred to PVDF membranes, followed by incubation with 5% nonfat dry milk (Cell Signaling Technology) for 1 h. After incubated with primary antibody overnight and secondary antibody for 1 h, membranes were developed with BCIP/NBT solution (Nacalai Tesque). The primary antibodies used in this study were as follows: ATF4 (#693901, BioLegend), FDFT1 (#13128-1-AP), GAPDH (#60004-1-Ig), and β-tubulin (#10094-1-AP) purchased from Proteintech,

ASNS (#sc-365809), vimentin (#sc-373717), and p53 (#sc-126) purchased from Santa Cruz Biotechnology and 4EBP1 (#9644), p-4EBP1 (#2855), p-Akt (#2965), p-c-Raf (#9421), p-MEK (#9154), p-ERK (#4370), p-P70S6K (#9234), p-S6 (#4858), GCN2 (#65981), p-GCN2 (#94668), eIF2α (#5324), p-eIF2α (#3398), LC3B (#3868), E-cadherin (#3195), and N-cadherin (#13116) purchased from Cell Signaling Technology. The secondary antibodies used were anti-rabbit IgG (Fc) AP conjugate (#S3738, Promega), anti-mouse IgG (H&L) AP conjugate (#S3728, Promega), and anti-rat IgG (H + L) AP conjugate (#S3831, Promega).

2.2.7 Autophagy assay

Autophagy in cells were observed by using CYTO-ID® Autophagy detection kit 2.0 (Enzo Life Sciences) marking autophagosomes. Cells were seeded on coverslips coated with Cellmatrix Type I-C (Nitta Gelatin) in a 24-well plate, and culture for 24 h. Then, cells were treated with Bis A for 48 h or CQ for 2 h. According to the instructions of CYTO-ID® Autophagy detection kit 2.0, cells were stained by CYTO-ID Green Detection Reagent 2 and Hoechst 33342 at the same time, followed by fixation of 4% paraformaldehyde for 20 min. All-in-One Fluorescence Microscope BZ-X800E (Keyence) was used to observe cells on the coverslip.

2.2.8 ROS level assay

ROS Assay Kit -Highly Sensitive DCFH-DA- (Dojindo) was used to determine the intracellular reactive oxygen species (ROS) level in cells. 2.5×10^4 A549 cells were

seeded in a 96-well clear black plate (clear bottom) for 24 h of incubation and subsequently, administrated by Bis A for 24 h or 48 h. Besides, as the positive control, hydrogen peroxide (100 μM) was added 30 min before performing ROS assay kit. EnVision Multimode Microplate Reader (PerkinElmer) was used to detect fluorescence signals, and All-in-One Fluorescence Microscope BZ-X800E was utilized to capture images.

2.2.9 Flow cytometer analysis

After exposure to Bis A for 72 h, cells were collected and subjected to washing with PBS as well as fixing with 70% ethanol saved at -20 °C. Cells were kept at -20 °C for 12 h, followed by washing with PBS and incubation with Ribonuclease (DNase-free) Glycerol Solution (Nippon Gene) at 37°C for 30 min. Next, cells were treated with 50 μg/mL propidium iodide (PI) (Nacalai Tesque) and analyzed by Gallios Flow Cytometer (Beckman Coulter).

2.2.10 Wound healing assay

A total of 2.0×10^5 A549 cells or 1.2×10^5 H1299 cells were seeded into a 24-well plate and cultured for 24 h. 200 μL tips were utilized for scratching a line at the bottom of wells that then, were washed by medium. After administration of Bis A, cells were observed under a microscopy (Olympus). ImageJ software (National Institutes of Health) was used to analyze the wound area.

2.2.11 Transwell-plate assay

Cell migration was determined by using a chamber of Chemotaxicell (Kurabo Industries) equipped with a polycarbonate membrane with an 8 μm pore size, as previous description [35]. 8×10^4 cells suspended in 200 μL of DMEM without FBS were seeded into a chamber that was put in a 500 μL of DMEM with 10% FBS in a well of a 24-well plate. Cells administrated by Bis A were culture for 24 h, and subsequently, the membrane experienced fixation of 20% MeOH and staining of 0.1% crystal violet. Cells on the upper side of the membrane were removed by Cotton swabs, followed by being observed under All-in-One Fluorescence Microscope BZ-X800E.

2.2.12 Measurement of Asn, GSH, and GSSG levels

8.0×10^5 cells per well were seeded into a 6-well plate for 24 h of incubation. After cells were treated with Bis A for 24 h or 48 h, culture medium was discarded and cells were washed with 5% (w/w) mannitol. Subsequently, cells were covered by methanol for 30 s, following by the addition of internal standard solution (Human Metabolome Technologies). The extract was centrifuged at 2300 × g, 4°C, for 5 min, and then the supernatant was centrifuged using an ultrafiltration tube (Ultrafree MC PLHCC, HMT, centrifugal filter unit 5 kDa) at 9100 × g, 4°C, for 2 h. Afterwards, Human Metabolome Technologies, Inc. performed the measurement of Asn, GSH and GSSG levels in cells. The filtrate was dried and dissolved again in Milli-Q water for measurement. Agilent CE-TOFMS system (Agilent Technologies) with a fused silica capillary i.d. 50 μm × 80 cm was used to determine the concentrations of Asn, GSH, and GSSG. The

measurement conditions were as follows: cation mode (run buffer: cation buffer, solution (p/n: H3301-1001), rinse buffer: cation buffer solution (p/n: H3301-1001), sample injection: pressure injection 50 mbar, 5 s, CE voltage: positive, 30 kV, MS ionization: ESI positive, MS capillary voltage: 4,000 V, MS scan range: m/z 50-1,000, sheath liquid: HMT sheath liquid (p/n: H3301-1020) and anion mode (run buffer: anion buffer solution (p/n: I3302-1023), rinse buffer: anion buffer solution (p/n: I3302-1023), sample injection: pressure injection 50 mbar, 10 s, CE voltage: positive, 30 kV, MS ionization: ESI negative, MS capillary voltage: 3,500 V, MS scan range: m/z 50–1,000, and sheath liquid: HMT sheath liquid (p/n: H3301-1020). For peaks detected by CE-TOFMS, automatic integration software MasterHands ver. obtained the charge ratios (m/z), peak area values, and migration times (MT). Using the peak area corrected by the internal standard substance for the calibration curve, the concentration was calculated for each substance as a one-point calibration of 100 μM (200 μM internal standard substance).

2.2.13 Transcriptome analysis

AmpliSeq Transcriptome Human Gene Expression Kit (Thermo Scientific) was used in the whole-transcriptome analysis. For library preparation, a barcoded cDNA library was first generated using the SuperScript VILO cDNA Synthesis kit (Thermo Fisher Scientific) from 10 ng of total RNA. Then, cDNA was amplified for 12 cycles by adding PCR Master Mix and the AmpliSeq human transcriptome gene expression primer pool (Thermo Fisher Scientific). After multiplex PCR, Ion Xpress Barcode Adapters

(Thermo Fisher Scientific) were ligated to the PCR products, which were then purified using Agencourt AMPure XP beads (Beckman Coulter). The purified libraries were pooled and then sequenced using an Ion Torrent S5 instrument and the Ion 550 Chip Kit (all from Thermo Fisher Scientific). The Ion Torrent Suite v5.12 software (Thermo Fisher Scientific) was used for base calling, alignment to the human reference genome (hg19), and quality control. Raw reads were then analyzed automatically using the AmpliSeqRNA plugin to generate gene-level expression values for all 20,802 RefSeq human genes. Gene Set Enrichment Analysis (GSEA) was performed to identify pathways enriched in the Molecular Signatures Database (MSigDB) Gene Ontology Biological Process (GObp) gene set [36]. A false discovery rate (FDR) q value of <0.25 and a nominal p value of <0.05 and were considered statistically significant.

2.2.14 Combination treatment analysis

CompuSyn software (ComboSyn) employing the Chou-Talalay method [37], was used to analyze the effect of combination treatment of Bis A and L-ASNase, torin-1, or rapamycin. Following the guide of users, the combination index (CI) values were calculated by using the fraction of affected cells (Fa) that is the inhibition rate of cells, of drug alone and combination. CI <1.0, =1.0 or >1.0 represents a synergistic effect, an additive effect, or antagonism, respectively.

2.2.15 Statistical analysis

The data were presented as mean ± SEM values of three or more than three independent

experiments and subjected to one-way ANOVA and Dunnett's multiple comparison tests by using the GraphPad Prism software. Statistical significance was determined at $P < 0.05$.

2.3 Results

2.3.1 Bis A suppresses cell proliferation of NSCLC cells

To determine the antiproliferation effect of Bis A, NSCLC A549 and H1299 cells were used. As shown in Figure 4A–C, Bis A not only suppressed the viability of 2D-culture of A549 cells with an IC_{50} of 1.7 μM, but also inhibited the viability of 3D-spheroid of A549 cells. Moreover, Bis A also exhibited similar inhibitory activities in H1299 cells (Figure 4D–F), which disclosed the anticancer effect of Bis A in NSCLC cells.

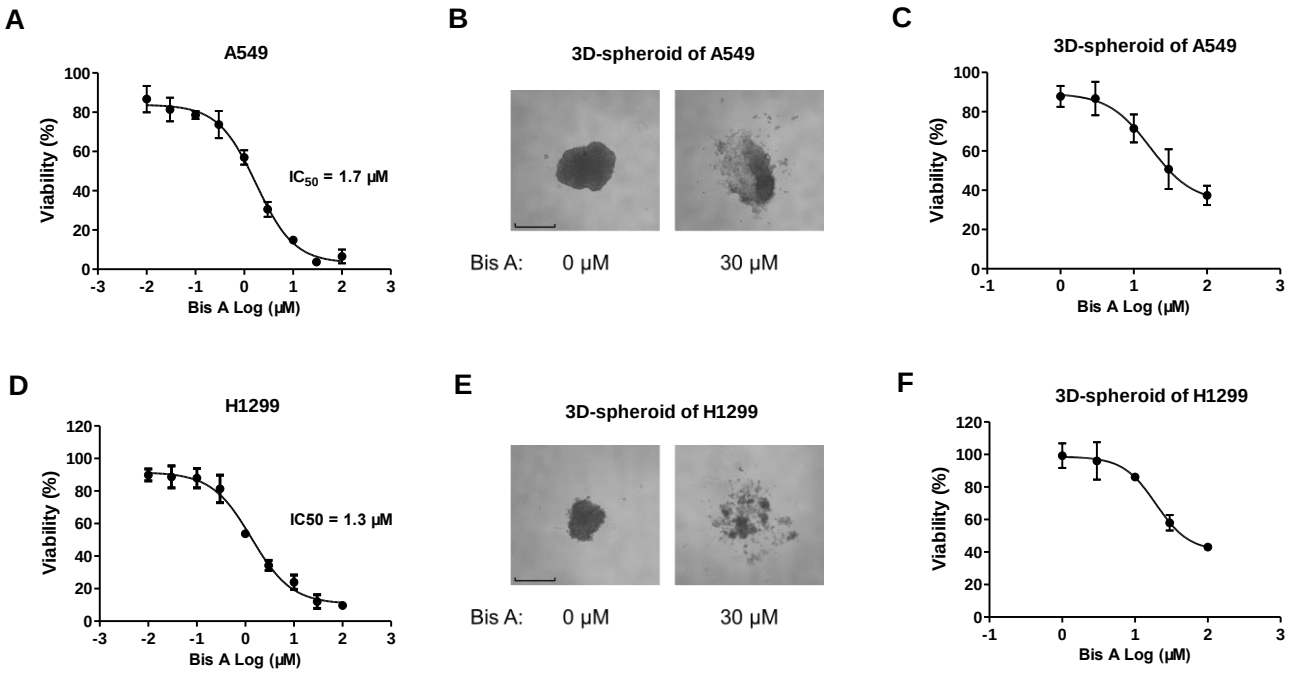

Figure 4. The effect of Bis A on the cell viability. (A) Viabilities of A549 cells (2D) after administration of Bis A for 72 h (n = 4). (B) The morphology of 3D-spheroid of A549 cells exposed to 0 or 30 μM Bis A for 72 h. The scale is 500 μm. (C) The viability of 3D-spheroid of A549 cells after treatment with Bis A for 72 h (n = 3). (D) The viability of H1299 cells (2D)

treated with Bis A for 72 h (n = 3). (E) The morphology of 3D-spheroid of H1299 cells after exposure to 0 or 30 μM Bis A for 72 h. The scale is 500 μm. (F) Viabilities of 3D-spheroid of H1299 cells administrated by Bis A for 72 h (n = 3). Data are represented as mean ± SEM.

2.3.2 Bis A targets ASNS in cells

To confirm Bis A targeting ASNS, at first, CETSA was executed. As shown in Figure 5A and B, Bis A could restrain the reduction of the band intensity of ASNS, along with the rise of temperature, which implied that Bis A could bind ASNS to avoid the precipitation of ASNS under high temperatures. Moreover, Bis A decreased the expression of ASNS (Figure 5C). A lower sensitivity of Bis A was observed in siASNS-transfected A549 cells or H1299 cells, compared with the findings in the siControl group (Figure 5D–G). In addition, Bis A could diminish the Asn level in A549 cells (Figure 5H), while the cell viability of A549 cells treated with Bis A, were rescued by the supplementation of Asn (Figure 5I). Taken together, these results suggested that Bis A could target ASNS to suppress cell proliferation.

As reported, the activity of microsomal squalene synthetase (SQS) prepared from HepG2 cells *in vitro* was inhibited by Bis A [18]. Therefore, the effect of Bis A on SQS in A549 cells were investigated. Nonetheless, a SQS inhibitor TAK-475, further decreased the viability of A549 cells exposed to Bis A (Figure 5J). Thereafter, siFDFT1 transfection was performed to reduce SQS expressions in cells, as the FDFT1 gene encodes the SQS protein (Figure 5K). siFDFT1-transfected cells did not display lower sensitivity to the antiproliferative activity of Bis A (Figure 5L). Therefore, these results indicated that Bis A did not target SQS in A549 cells.

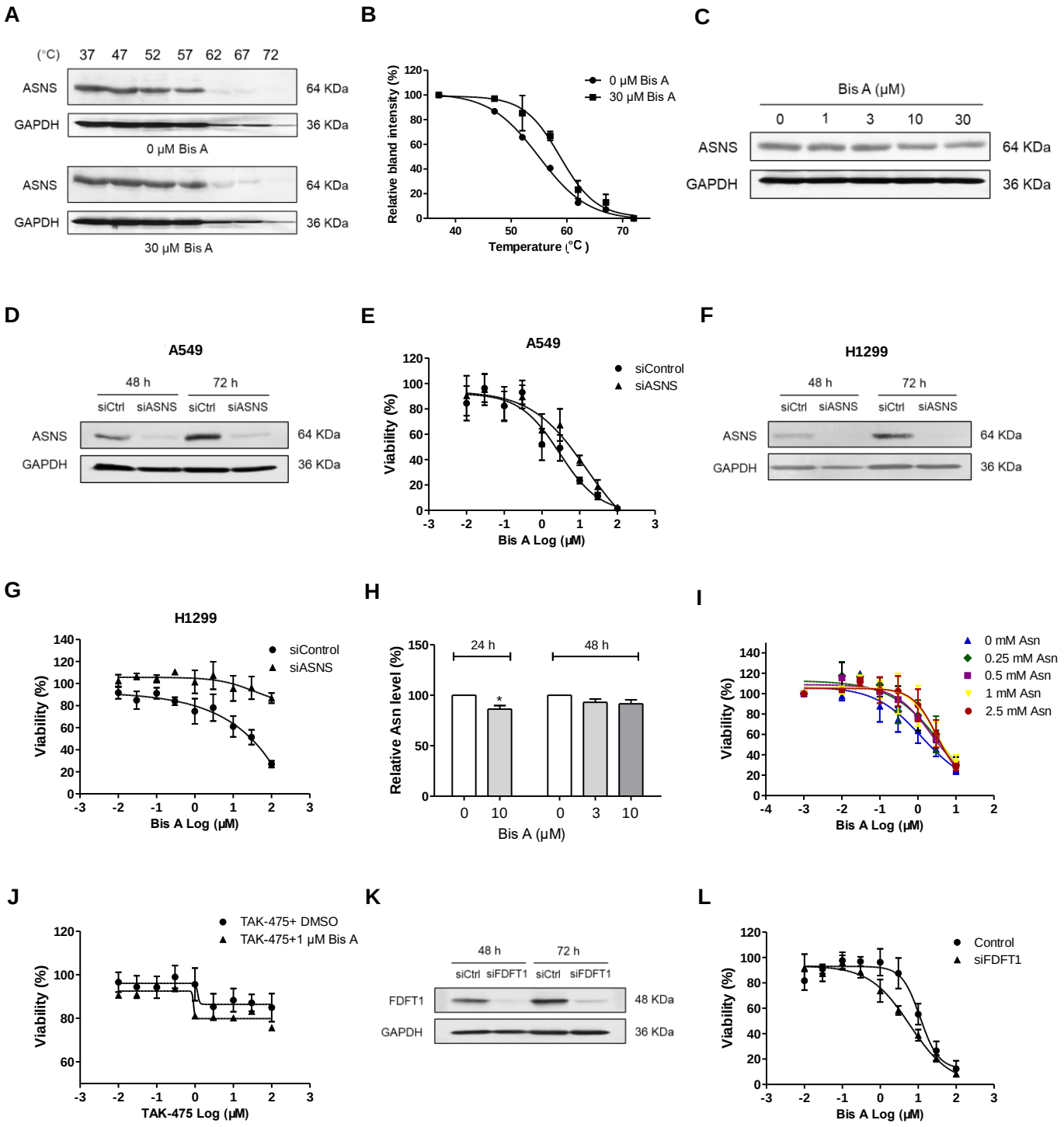

Figure 5. Bis A targets ASNS in cells. (A) Western blot of ASNS and GAPDH after CETSA. (B) The quantification of (A) (n = 3). (C) The ASNS expression in A549 cells administrated by Bis A for 48 h in western blot analysis (n= 4). (D) The protein expression of ASNS in A549 cells transfected with siControl(siCtrl) or siASNS for 48 h or 72 h. (E) Viabilities of siControl- or siASNS-transfected A549 cells after administration of Bis A for 48 h (n = 3). (F) The ASNS expression of siControl- (siCtrl-) or siASNS-transfected H1299 cells. (G) The viability of siControl- or siASNS-transfected H1299 cells after treatment with Bis A for 48 h (n = 3). (H)

Relative Asn level in A549 cells exposed to Bis A (n = 3). (I) The viability of A549 cells administrated by Bis A plus supplementation of Asn for 72 h. (J) The viability of A549 cells co-administered by TAK-475 and DMSO or 1 μM Bis A (n = 3). (K) FDFT1 expressions of A549 cells after siControl (siCtrl) or siASNS transfection. (L) Viabilities of siControl- or siFDFT1-transfected A549 cells after exposure to Bis A for 72 h (n = 3). Data are represented as mean ± SEM; P values were determined by one-way ANOVA with Dunnett's multiple comparisons test. *P < 0.05.

2.3.3 Effect of combination treatment of Bis A and L-ASNase

Because there is a promising anticancer strategy, decreasing the intracellular and extracellular levels of Asn at the same time, the effect of combination treatment of Bis A and L-ASNase was studied. As shown in Figure 4A, 6A and 6B, the alone treatment of Bis A or L-ASNase and their combination treatment significantly curbed the viability of A549 cells. Their combination effect was represented by the combination index (CI), after the analysis of CompuSyn. The CI value was lower than 1.0 could be observed when the fraction affected (Fa) was higher than or equal to 0.8 (Figure 6C and D), which revealed the synergistic effect of combination treatment of Bis A with L-ASNase in repressing the viability of A549 cells. Consequently, the results showed the potential of their combination treatment as chemotherapy strategy.

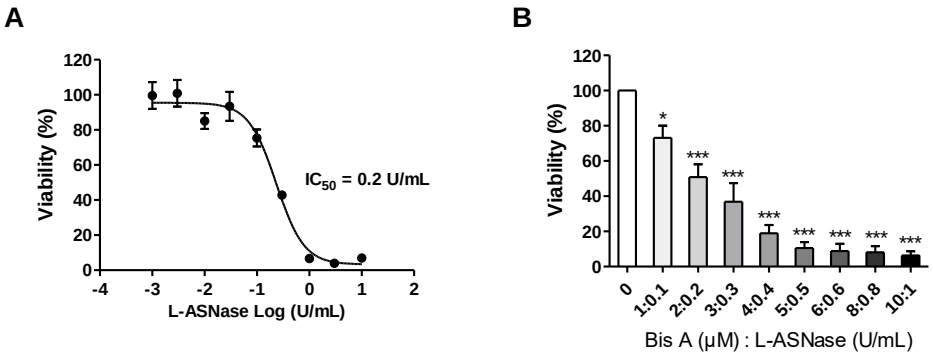

C

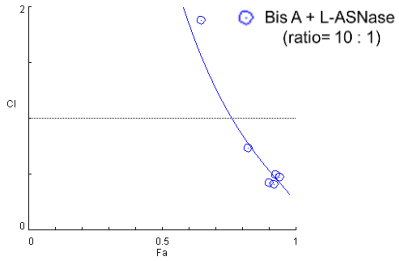

D

Fa	CI Value
0.7	1.26635
0.75	1.04162
0.8	0.84875
0.85	0.68118
0.9	0.53289
0.95	0.39538
0.97	0.33812

Figure 6. The effect of combination treatment with Bis A and L-ASNase. (A) The viability of A549 cells administered by L-ASNase for 72 h (n = 3). (B) The viability of A549 cells co-treated with Bis A and L-ASNase for 72 h (n = 3). (C) Fraction affected (Fa)-combination index (CI) plot results of combination treatment of Bis A (μM) and L-ASNase (U/mL). (D) The summary of Fa and corresponding CI values. The CI lower than 1.0 points out the synergism of the combination. Data are represented as mean ± SEM; P values were determined by one-way ANOVA with Dunnett's multiple comparisons test. *P < 0.05, ***P < 0.001.

2.3.4 Bis A activates GCN2-eIF2α-ATF4, PI3K-AKT-mTORC1, and RAF-MEK-ERK pathways

In contrast to the findings in the control group, the decreased Asn levels was observed in A549 cells after 24 h treatment with Bis A, but not found in treatment for 48 h (Figure 5H). The recovery trend suggested that Bis A may stimulate negative feedback pathways to change the intracellular Asn level. ATF4 is a transcription factor of ASNS, and the GCN2-eIF2α-ATF4 axis of AAR pathway was reported to hinder the antiproliferative activity of Asn depletion [29, 38]. Therefore, the related proteins in AAR pathway were focused on. As shown in Figure 7A and B, protein expressions of p-GCN2, p-eIF2α and ATF4 were elevated by Bis A, revealing the activation of Bis A on AAR pathway. Accordingly, AAR pathway was considered as a potential negative feedback pathway of Bis A treatment.

GSEA with GObp database was further used to analyze the transcriptome in A549

cells exposed to Bis A. The enrichment in PI3K signaling boosted by Bis A was observed, while enrichments in chemotaxis and migration were shown in the DMSO group ((Figure 7C and D). The stimulation of Bis A on PI3K-AKT-mTOR pathway was further indicated when Bis A enhanced protein levels of p-Akt, p-S6, p-P70S6K, and p-4E-BP1(Figure 7E and F). mTORC1 also could be activated by RAS-RAF-MEK-ERK pathway. Western blot analysis showed that the protein expression of p-c-Raf, p-MEK, and p-ERK was elevated by Bis A (Figure 7E and F). Due to the important contribution of mTORC1 activation on protein synthesis and cell proliferation [39], it was speculated that PI3K-AKT-mTOR and RAF-MEK-ERK pathways were correlated with the negative feedback regulation of Bis A.

Torin-1 is an mTORC1/2 inhibitor, and rapamycin is an mTORC1 inhibitor. The antiproliferative effect of Bis A were reinforced by torin-1 or rapamycin (Figure 7G). Furthermore, the combination treatment of Bis A with torin-1 or rapamycin exhibited synergistic effects (Figure 7H and I). These results further implied that the negative feedback regulation induced by PI3K-AKT-mTOR and RAF-MEK-ERK pathways impaired the anticancer activity of Bis A.

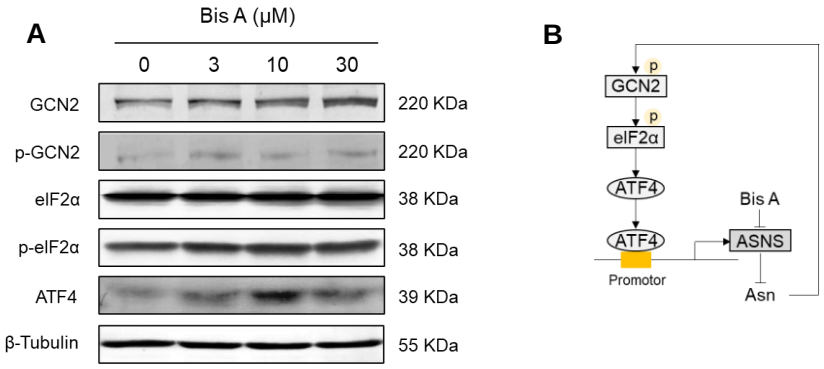

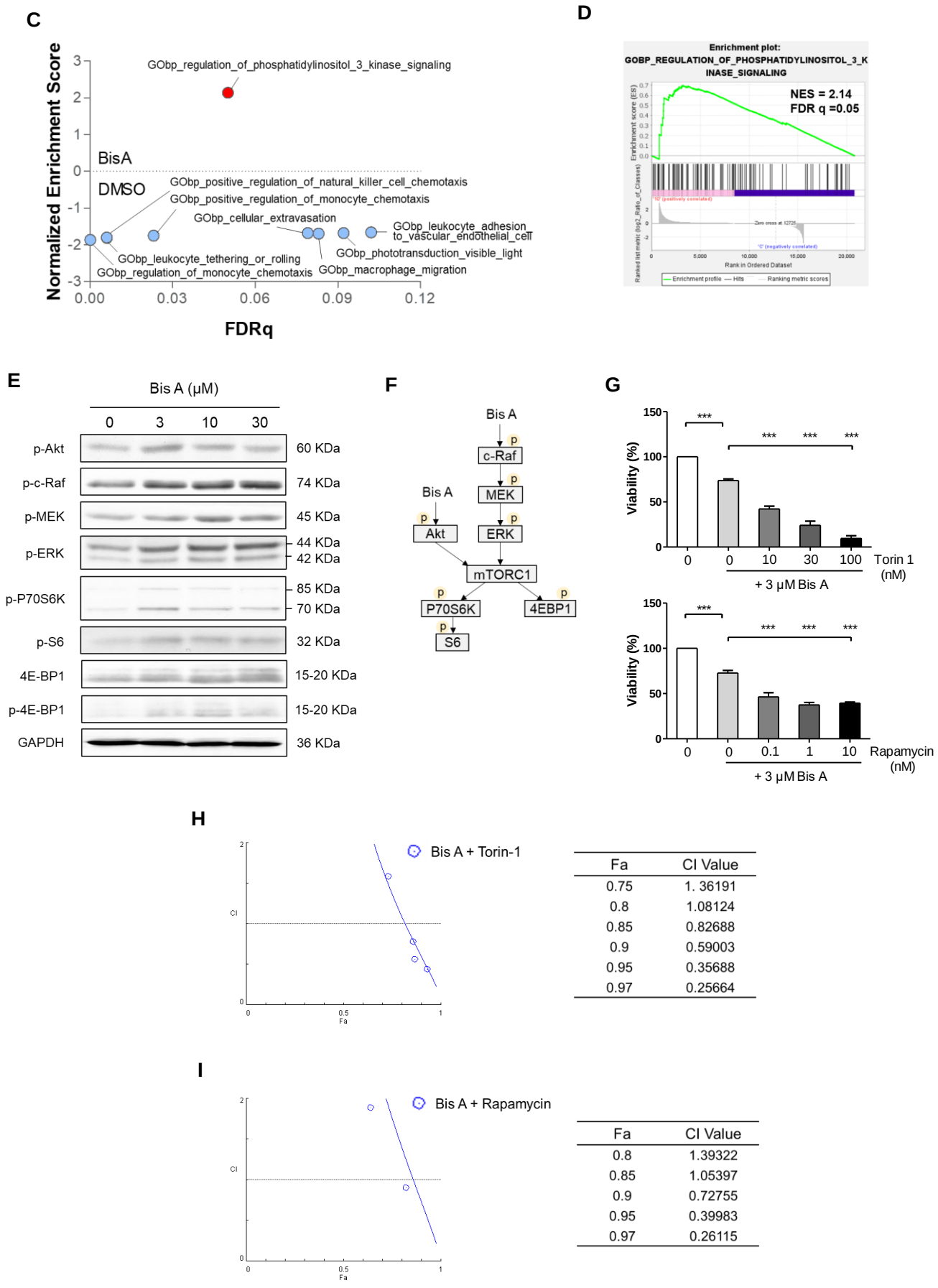

Figure 7. The signaling pathway regulated by Bis A. (A) The protein expression of GCN2,

p-GCN2, eIF2α, p-eIF2α, and ATF4 in A549 cells treated with Bis A for 48 h. (B) Schematic of the effect of Bis A on the AAR signaling pathway. (C) The result of GSEA, using the GObp database, of A549 cells exposed to DMSO or 10 μM Bis A for 6 h. The x-axis represents FDR q-value (FDRq) and the y-axis represents normalized enrichment score (NES). NES > 0 presents the Bis A-enrichment pathway, while NES < 0 presents the DMSO-enrichment pathway. (D) Positive enrichment of Bis A in PI3K signaling pathway. (E) The effect of Bis A on protein expressions of p-Akt, p-c-Raf, p-MEK, p-ERK, p-P70S6K, p-S6, 4E-BP1, and p-4E-BP1 in A549 cells. A549 cells were exposed to Bis A for 48 h. (F) Schematic exhibiting the effect of Bis A on PI3K-AKT-mTORC1 and RAF-MEK-ERK signaling pathways. (G) The viability of A549 cells after co-administration of Bis A with torin-1 or rapamycin for 72 h. The control group was A549 cells only exposed to 3 μM Bis A (n = 3). (H) Fa-CI plot results (left) and summary of Fa and corresponding CI values (right) of combination treatment with Bis A (μM) and torin-1 (nM) (the constant ratio was Bis A: torin-1 = 1:3). (I) Fa-CI plot results (left) and summary of Fa and corresponding CI values (right) of combination treatment with Bis A (μM) and rapamycin (nM) (the constant ratio was Bis A: rapamycin = 100:1). Data are represented as mean ± SEM; P values were determined by one-way ANOVA with Dunnett's multiple comparisons test. ***$P < 0.001$.

2.3.5 Bis A impedes autophagy and promotes oxidative stress and apoptosis

For obtaining sufficient nutrients to maintain rapid cell growth, cancer cells could induce autophagy [40, 41]. However, autophagy is inhibited by mTORC1 activation [39], and hence, the effect of Bis A on autophagy was researched. In the cytoplasm of A549 cells, Bis A obviously increased autophagosomes marked by green fluorescence (Figure 8A). This result was similar to the observation in the positive control group treated with CQ as an autophagy inhibitor impeding the degradation of autophagosome (Figure 8A). Besides, increased LC3B-II expressions were observed in A549 cells administrated by Bis A, but not were shown after the co-treatment of Bis A and CQ, which suggested that autophagosome degradation was hampered by Bis A (Figure 8B). Therefore, it is possible that Bis A inhibited autophagy through activating mTORC1

and precluding autophagosome degradation.

In response to nutrient depletion, impaired autophagy propelled accumulation of oxidative stress [42–44]. An antioxidant DL-α-tocopherol rescued the viability of A549 cells inhibited by Bis A (Figure 8C), suggesting that oxidative stress was associated to the antiproliferative effect of Bis A. Although in oxidative stress, tumorigenesis is affected by ROS, cell apoptosis could be induced by the cytotoxicity of ROS with high level [45]. Therefore, DCFH-DA was used to measure ROS levels in cells. As shown in Figure 8D and E, Bis A provoked more generation of ROS marked with green fluorescence in A549 cells. In addition, Bis A reduced levels of reduced glutathione (GSH), a crucial antioxidant to protect cells, to promote the production of oxidized glutathione (GSSG) (Figure 8F). In consequence, these results showed that Bis A triggered oxidative stress to exert antiproliferative activity in A549 cells.

Cell apoptosis could be caused by the inhibition of autophagy as well as oxidative stress, which was involved in the regulation of p53 protein, an important tumor suppressor [45–48]. In flow cytometer analysis, Bis A was observed to elevate the intensity of sub-G1 peak in A549 cells after 72 h treatment (Figure 8G), implying the effect of Bis A on cell apoptosis. This observation was further confirmed by the result that the antiproliferative activity of Bis A was obstructed by Z-VAD-FMK as a pan-caspase inhibitor (Figure 8H). In addition, as shown in Figure 8I, Bis A increased p53 expressions in A549 cells. Accordingly, it was inferred that Bis A may hinder autophagy and induce oxidative stress to encourage apoptosis, which involved p53 regulation.

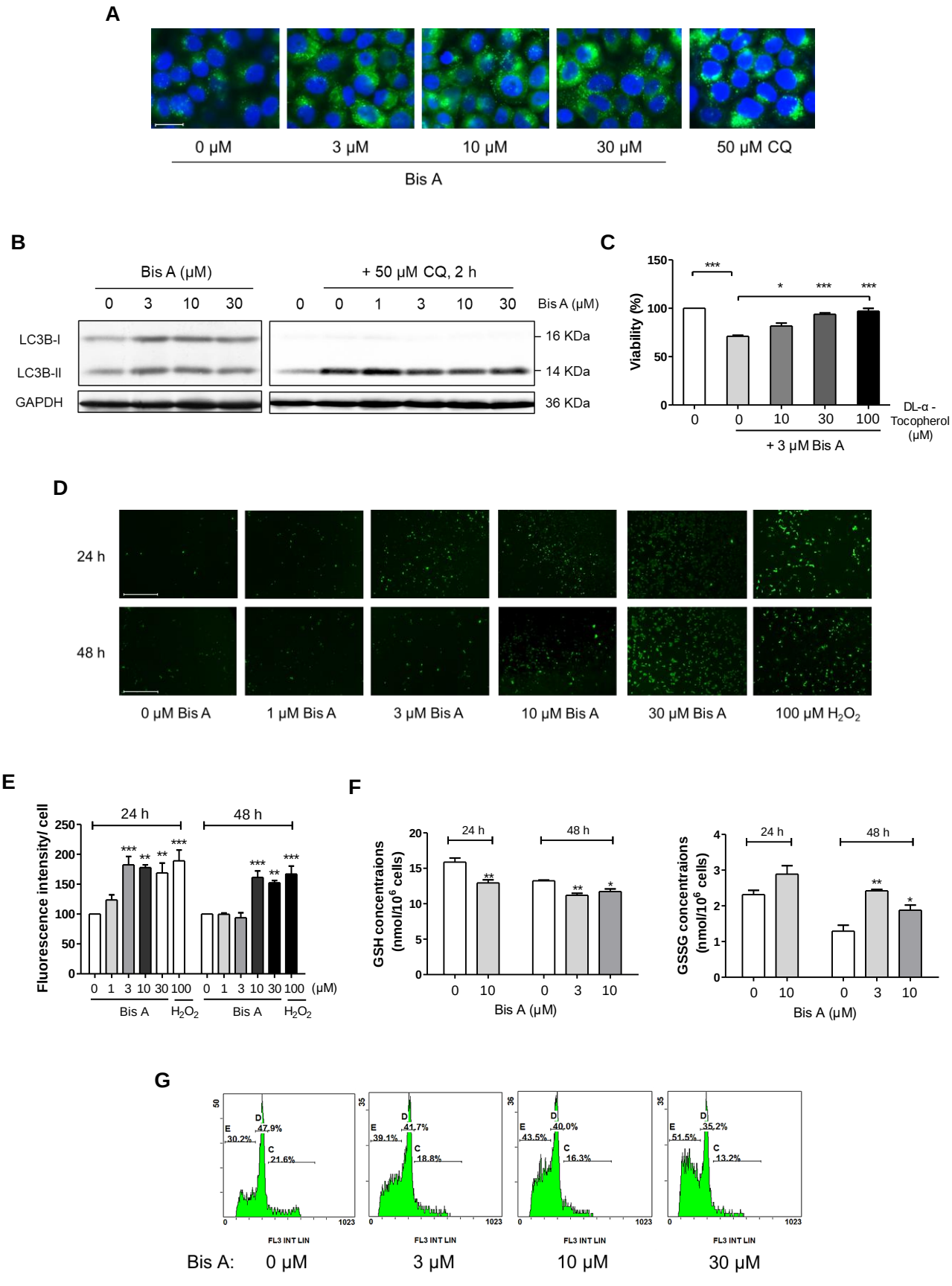
A
0 μM
3 μM
10 μM
30 μM
50 μM CQ
Bis A
B
Bis A (μM)
+ 50 μM CQ, 2 h
0 3 10 30
0 0 1 3 10 30
Bis A (μM)
LC3B-I
LC3B-II
GAPDH
16 KDa
14 KDa
36 KDa
C
Viability (%)
150
100
50
0
***
*
***
***
0 0 10 30 100
DL-α - Tocopherol (μM)
+ 3 μM Bis A
D
24 h
48 h
0 μM Bis A
1 μM Bis A
3 μM Bis A
10 μM Bis A
30 μM Bis A
100 μM H2O2
E
Fluorescence intensity/ cell
24 h
48 h
0 1 3 10 30 100 0 1 3 10 30 100 (μM)
Bis A
H2O2
Bis A
H2O2
F
GSH concentraions (nmol/10^6 cells)
24 h
48 h
0 10 0 3 10
Bis A (μM)
GSSG concentraions (nmol/10^6 cells)
24 h
48 h
0 10 0 3 10
Bis A (μM)
G
D 47.9%
E 30.2%
C 21.6%
D 41.7%
E 39.1%
C 18.8%
D 40.0%
E 43.5%
C 16.3%
D 35.2%
E 51.5%
C 13.2%
FL3 INT LIN
Bis A: 0 μM
3 μM
10 μM
30 μM

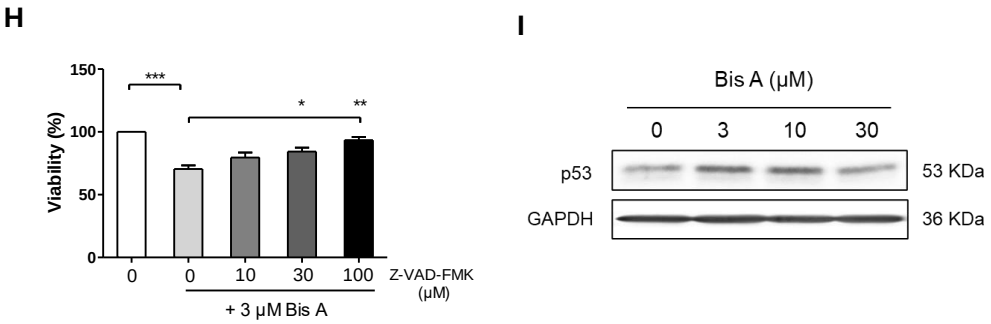

Figure 8. The effect of Bis A on autophagy, oxidative stress as well as cell apoptosis. (A) Images of merged fluorescence in A549 cells. A549 cells were exposed to Bis A for 48 h or CQ for 2 h. The fluorescence of blue and green indicates nucleus stained by Hoechst 33342 and autophagosomes labeled by CYTO-ID Green Detection Reagent 2, respectively. (B) Western blot of LC3B-II expressions in A549 cells after treatment with Bis A for 48 h with or without 50 μM CQ. (C) Viabilities of A549 cells after co-treatment of DL-α-tocopherol and 0 or 3 μM Bis A for 72 h. The control group was A549 cells only administrated by 3 μM Bis A (n = 3). (D) The image and (E) the fluorescence intensity of green fluorescence indicating ROS in A549 cells exposed to Bis A or H_2O_2 (n = 3 or 4). A549 cells treated with H_2O_2 for 30 min was regarded as the positive control. (F) GSH and GSSG concentrations in Bis A-treated A549 cells (n = 3). (G) The flow cytometer analysis of A549 cells administrated by Bis A for 72 h and stained with PI. (H) The viability of A549 cells after exposure to Z-VAD-FMK, with or without 3 μM Bis A for 72 h. The control group was A549 cells only treated with 3 μM Bis A (n = 3). (I) The protein expression of p53 in A549 cells after administration of Bis A for 48 h. Data are represented as mean ± SEM; P values were determined by one-way ANOVA with Dunnett's multiple comparisons test. *P < 0.05, **P < 0.01, and ***P < 0.001.

2.3.6 Bis A curbs cell migration and EMT

As shown in Figure 7C, Bis A was possible to have impacts on the cellular processes in cell migration and chemotaxis. Consequently, the effect of Bis A on cell migration were investigated by performing the wound healing assay and transwell-plate assay. In contrast to the findings in DMSO group, the wound closure was hindered by Bis A, in A549 cells and H1299 cells (Figure 9A and B). Moreover, Bis A restrained the migration of A549 cells through the chamber membrane (Figure 9C). TGF-β as a

cytokine triggering cell migration, could provoke EMT [49]. After treatment with 5 ng/mL of TGF-β, cell shape was altered, including becoming elongated and spindle-shaped, while decreased cell-cell contacts were displayed, but these changes could be recovered to some degree by Bis A (Figure 9D). Meanwhile, 5 ng/mL of TGF-β induced increased expressions of mesenchymal markers N-cadherin and vimentin, as well as decreased protein levels of the epithelial marker E-cadherin (Figure 9E). However, Bis A blocked these changes of protein expressions (Figure 9E). Accordingly, these results revealed the potential of Bis A on impeding EMT to hamper cell migration.

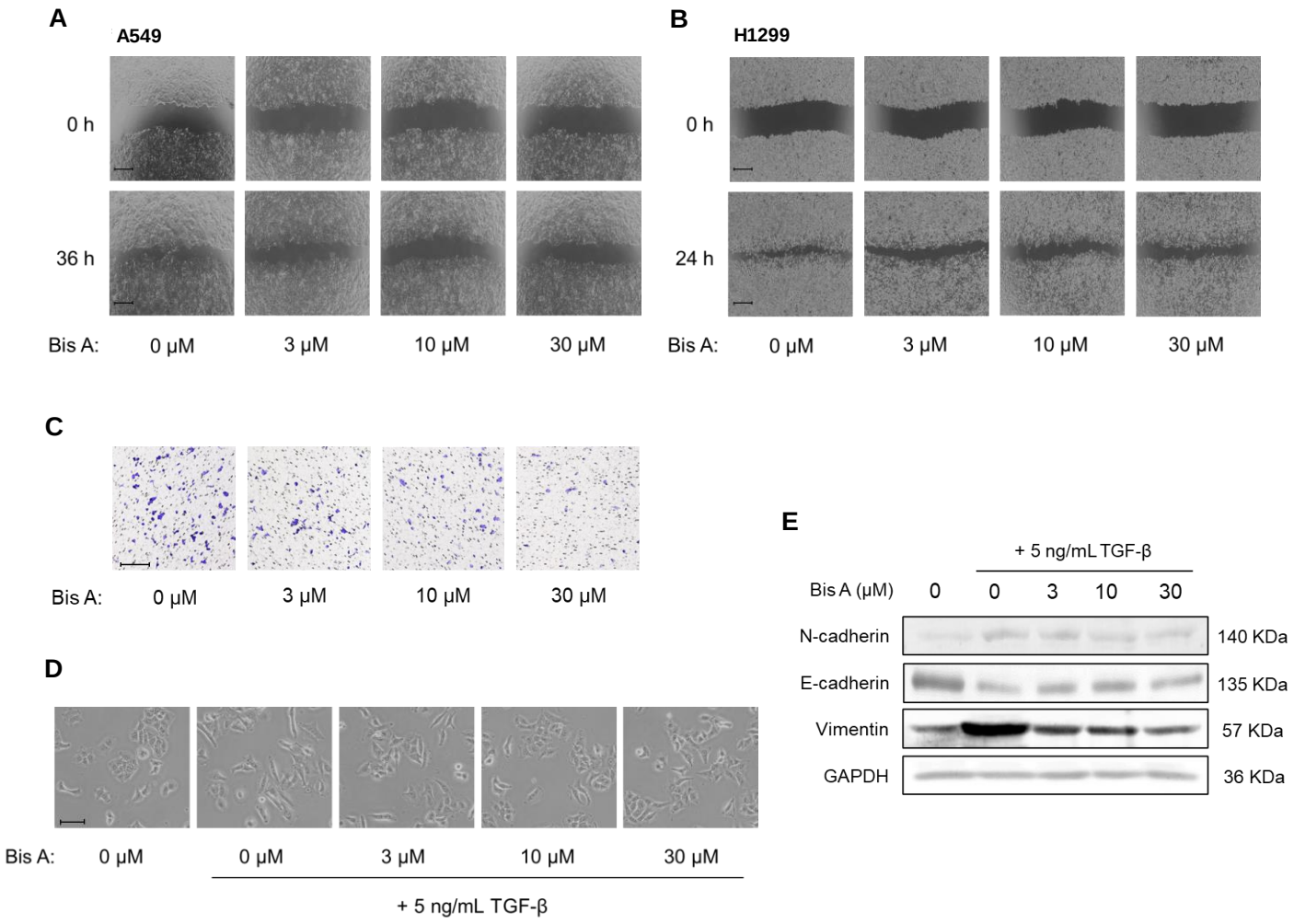

Figure 9. The effect of Bis A on cell migration and EMT. (A,B) The image of A549 cells (A) or H1299 cells (B) after scratch followed by administration of Bis A. The scale is 500 μm. (C)

Images of cells passing through the membrane of the chamber after treatment with Bis A for 24 h. The scale is 200 μm. (D) The morphology of A549 cells exposed to 5 ng/mL TGF-β, with or without Bis A for 24 h. The scale is 200 μm. (E) Protein expressions of N-cadherin, E-cadherin, and vimentin in A549 cells treated with 5 ng/mL TGF-β, with or without Bis A for 24 h.

2.4 Discussion

This chapter exhibited the anticancer effect and mechanism of Bis A. As an ASNS inhibitor, Bis A suppressed the viability of 2D-culture or 3D-spheroid of NSCLC A549 cells and H1299 cells (Figure 4), as well as targeting ASNS in these two cell lines (Figure 5). Bis A decreased Asn levels and the supplementation of Asn rescued the cell viability inhibited by Bis A (Figure 5H and I). However, under longer administration for 48 h, intracellular Asn level was similar to that in DMSO group (Figure 5H). AAR pathway, a response to nutritional stress [38], was induced by Bis A and was considered to further upregulate Asn levels as a negative feedback pathway (Figure 7A and B). Another factor may be the influx of extracellular Asn, but it requires further research on the effect of Bis A on several transporters using Asn as substrate, including ASCT2 and SNAT3 [11]. In addition, Asn as an amino acid exchange factor, was involved in uptake of some amino acids, while ATF4, a transcription factor of ASNS, affects serine synthesis pathway to regulate Asn levels in cells [30]. Accordingly, the way involves in Bis A regulating Asn levels need further detailed study.

Asn plays an important role in cancer progression, and even it was reported to rescue apoptosis triggered by Gln deprivation [50]. Considering the supplementation from extracellular Asn, L-ASNase with ability of depleting extracellular Asn, was used with Bis A to curb Asn levels in cells. Our study showed the synergistic effect of

combination treatment of Bis A and L-ASNase (Figure 6), which disclosed that reducing the intracellular and extracellular levels of Asn is a prospective anticancer therapy for ALL as well as solid cancers.

mTORC1 is a vital regulator of cell growth and metabolism. The activation of AAR pathway or mTORC1 is conducive to cancer development [38, 39]. In this study, Bis A provoked not only AAR pathway, but also PI3K-AKT-mTORC1 and RAF-MEK-ERK pathways (Figure 7), which was regarded as the potential negative feedback regulation. Apart from that, mTOR inhibitors rapamycin and torin-1, obviously reinforced the antiproliferative activity of Bis A (Figure 7G), as well as exhibited the synergistic effect with Bis A (Figure 7H and I), emerging the possibility of combining Bis A with mTOR inhibitors as a potential therapy.

Autophagy has cross-talk with ROS in cell signaling such as nutrition stress [42–44]. p53 involves in regulating autophagy, and it is a transcriptional sensor of ROS [42, 51]. It was observed that Bis A enhanced oxidative stress, apoptosis and p53 expressions, while inhibited autophagy flux by blocking autophagy induction as well as autophagosome degradation, in this study (Figure 8). Therefore, this revealed that there are close correlations among autophagy, oxidative stress, and apoptosis in the anticancer effect of Bis A. TGF-β-induced EMT and cell invasion required the involvement of autophagy [52–54]. Bis A was exhibited to obstruct cell migration and reverse EMT caused by TGF-β (Figure 9), suggesting that autophagy inhibition and oxidative stress induced by Bis A may influence the migration of NSCLC cells.

Summary

This study identified a new ASNS inhibitor, Bis A, with unique pharmacophore and binding site against ASNS, and for the first time, revealed K556 site on ASNS had the potential to affect the efficacy of the ASNS inhibitor. In mechanism, Bis A targeted ASNS in cells and exerted anticancer activity through promoting oxidative stress and apoptosis, while impeding autophagy, cell migration and EMT. Thus, Bis A could be a promising lead molecule in development of ASNS inhibitors. Additionally, the synergistic effect of Bis A with L-ASNase or the mTOR inhibitor showed a prospective strategy for cancer chemotherapy.

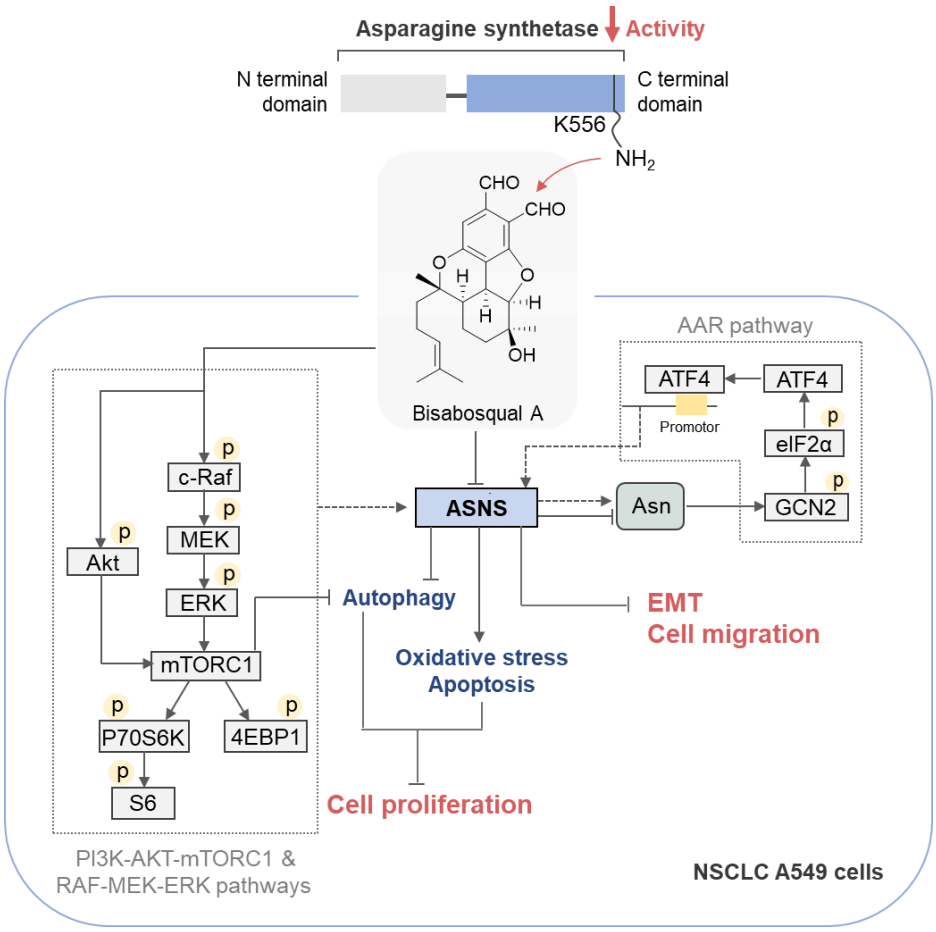

Figure 10. Proposed model. Diagram shows how Bis A inhibits the ASNS activity, and the anticancer effect of Bis A in NSCLC A549 cells.

Chapter 1 Identification of bisabosqual A as a potential ASNS inhibitor and investigation of the binding site of bisabosqual A on ASNS

An *in vitro* screening system was constructed using a purified recombinant hASNS to evaluate ASNS activities. By executing this system to screen our *in-house* microbial metabolite library, a unique bisabolane-type meroterpenoid molecule Bis A, produced by the fungus *Stachybotrys* sp. RF-7260, was identified as a potential ASNS inhibitor. Moreover, the study of structure-activity relationship among Bis A, and its analogs bisabosquals B, C, and D, further confirmed that Bis A was a promising hit molecule. Thereafter, the binding mode and binding site of Bis A on ASNS were investigated, and Bis A was observed to covalently bind to K556 site on ASNS *via* Schiff-base formation. The K556 site on ASNS exhibited the importance to ASNS inhibitory activity of Bis A, implying, for the first time, the possibility of K556 site to affect efficacy of ASNS inhibitors.

Chapter 2 Anticancer effect and mechanism of bisabosqual A in non-small cell lung cancer cells

In order to determine the anticancer effect of Bis A, NSCLC A549 and H1299 cells were used. Bis A could significantly inhibit the cell viability of not only 2D-culture but also 3D-spheroid of A549 cells or H1299 cells, and could target ASNS in both of these two cell lines. In addition, our results revealed the synergistic effect of Bis A and L-ASNase, an enzyme depleting extracellular Asn, in impeding cell proliferation.

In mechanism, Bis A was shown to activate GCN2-eIF2α-ATF4, PI3K-AKT-

mTORC1 as well as RAF-MEK-ERK pathways, as the negative feedback regulation. Besides, the combination treatment of Bis A and the mTOR inhibitor, torin-1 or rapamycin, exhibited synergistic effects in antiproliferative activity. Furthermore, our study showed that Bis A inhibited autophagy and induced oxidative stress and apoptosis in A549 cells. Bis A could impede cell migration, while restrain EMT triggered by TGF-β by reducing the expression of N-cadherin and vimentin, and enhancing the expression of E-cadherin.

Acknowledgements

First of all, I would like to express my heartfelt gratitude for the guidance and care from my supervisor, professor Hideaki Kakeya. I appreciate his expertise and efficiency, and his patience as well as encouragement have helped me overcome many challenges. I am also sincerely grateful for his support and assistance with my scholarship application. I am deeply thankful to associate professor Akira Hattori who provided professional guidance, enabling me to gain invaluable research experience. Every discussion and exchange with him provided me an opportunity for academic growth.

I would like to thank every member in my lab, especially Dr. Hiroaki Ikeda, Ms. Minori Inoue, Mr. Yoshiki Shiratsuchi, Ms. Haruka Ito, and Ms. Ai Koyama. Their assistance in my experiments and affairs in lab made my research more smoothly and effective.

I am greatly indebted to Prof. Kazuto Nishio and Dr. Kazuko Sakai of Kindai University, Dr. Naoshi Dohmae and Dr. Takehiro Suzuki of RIKEN, and Dr. Yoshinori Hirano of Keio University, for their profound contribution to this study.

I extend my sincere gratitude to Kyoto University Graduate Division and Japan Science and Technology Agency (JST), providing scholarship and research grant, as well as Otsuka Toshimi Scholarship Foundation, providing scholarship for me, which allowed me to focus more on research.

Finally, I would like to express my deepest thanks to my family, who have been my steadfast support, throughout my academic journey. Their understanding, encouragements, and support are my most precious treasures.

References

[1] Avramis, V.I., 2015. Asparagine synthetase polymorphisms and toxicity and efficacy of asparaginases. *Clin. Cancer Res.* 21, 230–232. https://doi.org/10.1158/1078-0432.CCR-14-1714.

[2] Zhu, W., Radadiya, A., Bisson, C., Wenzel, S., Nordin, B.E., Martínez-Márquez, F., Imasaki,T., Sedelnikova, S.E., Coricello, A., Baumann, P., Berry, A.H., Nomanbhoy, T.K., Kozarich, J.W., Jin, Y., Rice, D.W., Takagi, Y., Richards, N.G.J., 2019. High-resolution crystal structure of human asparagine synthetase enables analysis of inhibitor binding and selectivity. *Commun. Biol.* 2, 345. https://doi.org/10.1038/s42003-019-0587-z.

[3] Lomelino, C.L., Andring, J.T., McKenna, R., Kilberg, M.S., 2017. Asparagine synthetase: function, structure, and role in disease. *J. Biol. Chem.* 292, 19952–19958. https://doi.org/ 10.1074/jbc.R117.819060.

[4] Gwinn, D.M., Lee, A.G., Briones-Martin-del-Campo, M., Conn, C.S., Simpson, D.R., Scott, A.I., Le, A., Cowan, T.M., Ruggero, D., Sweet-Cordero, E.A., 2018. Oncogenic KRAS regulates amino acid homeostasis and asparagine biosynthesis via ATF4 and alters sensitivity to L-asparaginase. *Cancer Cell.* 33, 91–107. https://doi.org/10.1016/j.ccell.2017.12.003.

[5] Butler, M., van der Meer, L.T., van Leeuwen, F.N., 2021. Amino acid depletion therapies: starving cancer cells to death. *Trends Endocrin. Met.* 32, 367–381. https://doi.org/10.1016/j.tem.2021.03.003.

[6] Altman, B.J., Stine, Z.E., Dang, C.V., 2016. From Krebs to clinic: glutamine metabolism to cancer therapy. *Nat. Rev. Cancer* 16, 619–634. https://doi.org/10.1038/nrc.2016.71.

[7] Cramer, S.L., Saha, A., Liu, J., Tadi, S., Tiziani, S., Yan, W., Triplett, K., Lamb, C., Alters, S.E., Rowlinson, S., Zhang, Y.J., Keating, M.J., Huang, P., DiGiovanni, J., Georgiou, G., Stone, E., 2017. Systemic depletion of L-cyst(e)ine with cyst(e)inase increases reactive oxygen species and suppresses tumor growth. *Nat. Med.* 23, 120–127. https://doi.org/10.1038/nm.4232.

[8] Marini, B.L., Perissinotti, A.J., Bixby, D.L., Brown, J., Burke, P.W., 2017. Catalyzing improvements in ALL therapy with asparaginase. *Blood Rev.* 31, 328–338. https://doi.org/10.1016/j.blre.2017.06.002.

[9] Jiang, J., Batra, S., Zhang, J., 2021. Asparagine: a metabolite to be targeted in cancers. *Metabolites.* 11, 402. https://doi.org/10.3390/metabo11060402.

[10] Ren, Y., Roy, S., Ding, Y., Iqbal, J., Broom, J.D., 2004. Methylation of the asparagine synthetase promoter in human leukemic cell lines is associated with a specific methyl binding protein. *Oncogene.* 23, 3953–3961. https://doi.org/10.1038/sj.onc.1207498.

[11] Chiu, M., Taurino, G., Bianchi, M.G., Kilberg, M.S., Bussolati, O., 2020. Asparagine synthetase in cancer: beyond acute lymphoblastic leukemia. *Front. Oncol*. 9, 1480. https://doi.org/10.3389/fonc.2019.01480.

[12] Nishikawa, G., Kawada, K., Hanada, K., Maekawa, H., Itatani, Y., Miyoshi, H., Taketo, M.M., Obama, K., 2022. Targeting asparagine synthetase in tumorgenicity

using patient-derived tumor-initiating cells. *Cells.* 11, 3273. https://doi.org/10.3390/cells11203273.

[13] Richards, N.G.J., Kilberg, M.S., 2006. Asparagine synthetase chemotherapy. *Annu. Rev. Biochem.* 75, 629–654. https://doi.org/10.1146/annurev.biochem.75.103004.142520.

[14] Koroniak, L., Ciustea, M., Gutierrez, J.A., Richards, N.G.J., 2003. Synthesis and characterization of an N-acylsulfonamide inhibitor of human asparagine synthetase. *Org. Lett.* 5, 2033–2036. https://doi.org/10.1021/ol034212n.

[15] Ikeuchi, H., Ahn, Y.M., Otokawa, T., Watanabe, B., Hegazy, L., Hiratake, J., Richards, N.G.J., 2012. A sulfoximine-based inhibitor of human asparagine synthetase kills L-asparaginase-resistant leukemia cells. *Bioorg. Med. Chem.* 20, 5915–5927. https://doi.org/10.1016/j.bmc.2012.07.047.

[16] Hu, D., Yang, C., Lok, C.N., Xing, F., Lee, P.Y., Fung, Y.M.E., Jiang, H., Che, C.M., 2019. An antitumor bis(N-heterocyclic carbene)platinum(II) complex that engages asparagine synthetase as an anticancer target. *Angew. Chem. Int. Ed.* 58, 10914–10918. https://doi.org/10.1002/anie.201904131.

[17] Gutierrez, J.A., Pan, Y.X., Koroniak, L., Hiratake, J., Kilberg, M.S., Richards, N.G.J., 2006. An inhibitor of human asparagine synthetase suppresses proliferation of an L-asparaginase-resistant leukemia cell line. *Chem. Biol.* 13, 1339–1347. https://doi.org/10.1016/j.chembiol.2006.10.010.

[18] Minagawa, K., Kouzuki, S., Nomura, K., Yamaguchi, T., Kawamura, Y., Matsushima, K., Tani, H., Ishii, K., Tanimoto, T., Kamigauchi, T., 2001. Bisabosquals,

novel squalene synthase inhibitors – I. Taxonomy, fermentation, isolation and biological activities. *J. Antibiot.* 54, 890–895. https://doi.org/10.7164/antibiotics.54.890.

[19] Jumper, J., Evans, R., Pritzel, A., Green, T., Figurnov, M., Ronneberger, O., Tunyasuvunakool, K., Bates, R., Žídek, A., Potapenko, A., Bridgland, A., Meyer, C., Kohl, S.A.A., Ballard, A.J., Cowie, A., Romera-Paredes, B., Nikolov, S., Jain, R., Adler, J., Back, T., Petersen, S., Reiman, D., Clancy, E., Zielinski, M., Steinegger, M., Pacholska, M., Berghammer, T., Bodenstein, S., Silver, D., Vinyals, O., Senior, A.W., Kavukcuoglu, K., Kohli, P., Hassabis, D., 2021. Highly accurate protein structure prediction with AlphaFold. *Nature* 596, 583–589. https://doi.org/10.1038/s41586-021-03819-2.

[20] Varadi, M., Anyango, S., Deshpande, M., Nair, S., Natassia, C., Yordanova, G., Yuan, D., Stroe, O., Wood, G., Laydon, A., Žídek, A., Green, T., Tunyasuvunakool, K., Petersen, S., Jumper, J., Clancy, E., Green, R., Vora, A., Lutfi, M., Figurnov, M., Cowie, A., Hobbs, N., Kohli, P., Kleywegt, G., Birney, E., Hassabis, D., Velankar, S., 2022. AlphaFold protein structure database: massively expanding the structural coverage of protein-sequence space with high-accuracy models. *Nucleic Acids Res.* 50, D439–D444. https://doi.org/10.1093/nar/gkab1061.

[21] Schrödinger Release 2020-1: Schrödinger, LLC, New York, NY, 2020.

[22] Warshaviak, D.T., Golan, G., Borrelli, K.W., Zhu, K., Kalid, O., 2014. Structure-based virtual screening approach for discovery of covalently bound ligands. *J. Chem. Inf. Model*. 54, 1941–1950. https://doi.org/10.1021/ci500175r.

[23] Zhu, K., Borrelli, K.W., Greenwood, J.R., Day, T., Abel, R., Farid, R.S., Harder, E., 2014. Docking covalent inhibitors: a parameter free approach to pose prediction and scoring. *J. Chem. Inf. Model*. 54, 1932–1940. https://doi.org/10.1021/ci500118s.

[24] Kakeya, H., 2016. Natural products-prompted chemical biology: phenotypic screening and a new platform for target identification. *Nat. Prod. Rep*. 33, 648–654. https://doi.org/10.1039/c5np00120j.

[25] Ikeuchi, H., Meyer, M.E., Ding, Y., Hiratake, J., Richards, N.G.J., 2009. A critical electrostatic interaction mediates inhibitor recognition by human asparagine synthetase. *Bioorg. Med. Chem*. 17, 6641–6650. https://doi.org/10.1016/j.bmc.2009.07.071.

[26] Yang, T., Xiong, Y., Zeng, Y., Wang, Y., Zeng, J., Liu, J., Xu, S., Li, L.S., 2022. Current status of immunotherapy for non-small cell lung cancer. *Front. Pharmacol.* 13, 989461. https://doi.org/10.3389/fphar.2022.989461.

[27] Xu, Y., Lv, F., Zhu, X., Wu, Y., Shen, X., 2016. Loss of asparagine synthetase suppresses the growth of human lung cancer cells by arresting cell cycle at G0/G1 phase. *Cancer Gene Ther.* 23, 287–294. https://doi.org/10.1038/cgt.2016.28.

[28] Cai, D., Zhang, Z., Bu, Y., Li, L., Deng, Y., Sun, L., Hu, C., Li, M., 2022. Asparagine synthetase regulates lung-cancer metastasis by stabilizing the β-catenin complex and modulating mitochondrial response. *Cell Death Dis.* 13, 566. https://doi.org/10.1038/s41419-022-05015-0.

[29] Balasubramanian, M.N., Butterworth, E.A., Kilberg, M.S., 2013. Asparagine synthetase: regulation by cell stress and involvement in tumor biology. *Am. J. Physiol. Endocrinol. Metab*. 304, E789–E799. https://doi.org/10.1152/ajpendo.00015.2013.

[30] Krall, A.S., Xu, S., Graeber, T.G., Braas, D., Christofk, H.R., 2016. Asparagine promotes cancer cell proliferation through use as an amino acid exchange factor. *Nat. Commun*. 7, 11457. https://doi.org/10.1038/ncomms11457.

[31] Knott, S.R.V., Wagenblast, E., Khan, S., Kim, S.Y., Soto, M., Wagner, M., Turgeon, M.O., Fish, L., Erard, N., Gable, A.L., Maceli, A.R., Dickopf, S., Papachristou, E.K., D'Santos, C.S., Carey, L.A., Wilkinson, J.E., Harrell, J.C., Perou, C.M., Goodarzi, H., Poulogiannis, G., Hannon, G.J., 2018. Asparagine bioavailability governs metastasis in a model of breast cancer. *Nature*. 554, 378–381. https://doi.org/10.1038/nature25465.

[32] Fang, K., Chu, Y., Zhao, Z., Li, Q., Li, H., Chen, T., Xu, M., 2020. Enhanced expression of asparagine synthetase under glucose-deprived conditions promotes esophageal squamous cell carcinoma development. *Int J Med Sci.* 17, 510–516. https://doi.org/10.7150/ijms.39557.

[33] Selby, M., Delosh, R., Laudeman, J., Ogle, C., Reinhart, R., Silvers, T., Lawrence, S., Kinders, R., Parchment, R., Teicher, B.A., Evans, D.M., 2017. 3D models of the NCI60 cell lines for screening oncology compounds. *SLAS Discov.* 22, 473–483. https://doi.org/10.1177/2472555217697434.

[34] Molina, D.M., Jafari, R., Ignatushchenko, M., Seki, T., Larsson, E.A., Dan, C., Sreekumar, L., Cao, Y., Nordlund, P., 2013. Monitoring drug target engagement in cells and tissues using the cellular thermal shift assay. *Science.* 341, 84–87. https://doi.org/10.1126/science.1233606.

[35] Kume, K., Satomura, K., Nishisho, S., Kitaoka, E., Yamanouchi, K., Tobiume, S., Nagayama, M., 2002. Potential Role of Leptin in Endochondral Ossification. *J. Histochem. Cytochem.* 50, 159–169. https://doi.org/10.1177/002215540205000204.

[36] Mootha, V.K., Lindgren, C.M., Eriksson, K., Subramanian, A., Sihag, S., Lehar, J., Puigserver, P., Carlsson, E., Ridderstråle, M., Laurila, E., Houstis, N., Daly, M.J., Patterson, N., Mesirov, J.P., Golub, T.R., Tamayo, P., Spiegelman, B., Lander, E.S., Hirschhorn, J.N., Altshuler, D., Groop, L.C., 2003. PGC-1alpha-responsive genes involved in oxidative phosphorylation are coordinately downregulated in human diabetes. *Nat. Genet*. 34, 267–273. https://doi.org/10.1038/ng1180.

[37] Chou, T., 2010. Drug combination studies and their synergy quantification using the Chou-Talalay method. *Cancer Res.* 70, 440–446. https://doi.org/10.1158/0008-5472.CAN-09-1947.

[38] Ye, J., Kumanova, M., Hart, L.S., Sloane, K., Zhang, H., De Panis, D.N., Bobrovnikova-Marjon, E., Diehl, J.A., Ron, D., Koumenis, C., 2010. The GCN2-ATF4 pathway is critical for tumour cell survival and proliferation in response to nutrient deprivation. *EMBO J*. 29, 2082–2096. https://doi.org/10.1038/emboj.2010.81.

[39] Popova, N.V., Jücker, M., 2021. The role of mTOR signaling as a therapeutic target in cancer. *Int. J. Mol. Sci*. 22, 1743. https://doi.org/10.3390/ijms22041743.

[40] Kimmelman, A.C., White, E., 2017. Autophagy and tumor metabolism. *Cell Metab*. 25, 1037–1043. https://doi.org/10.1016/j.cmet.2017.04.004.

[41] Poillet-Perez, L., White, E., 2019. Role of tumor and host autophagy in cancer metabolism. *Genes & Dev*. 33, 610–619. https://doi.org/10.1101/gad.325514.119.

[42] Lee, J., Giordano, S., Zhang, J., 2012. Autophagy, mitochondria and oxidative stress: cross-talk and redox signalling. *Biochem. J.* 441, 523–540. https://doi.org/10.1042/BJ20111451.

[43] Filomeni, G., Zio, D.D., Cecconi, F., 2015. Oxidative stress and autophagy: the clash between damage and metabolic needs. *Cell Death Differ*. 22, 377–388. https://doi.org/10.1038/cdd.2014.150.

[44] Mizushima, N., Levine, B., Cuervo, A.M., Klionsky, D.J., 2008. Autophagy fights disease through cellular self-digestion. *Nature*. 451, 1069–1075. https://doi.org/10.1038/nature06639.

[45] Hayes, J.D., Dinkova-Kostova, A.T., Tew, K.D., 2020. Oxidative stress in cancer. *Cancer Cell*. 38, 167–197. https://doi.org/10.1016/j.ccell.2020.06.001.

[46] Bieging, K.T., Mello, S.S., Attardi, L.D., 2014. Unravelling mechanisms of p53-mediated tumour suppression. *Nat. Rev. Cancer*. 14, 359–370. https://doi.org/10.1038/nrc3711.

[47] Ceder, S., Eriksson, S.E., Liang, Y.Y., Cheteh, E.H., Zhang, S.M., Fujihara, K.M., Bianchi, J., Bykov, V.J.N., Abrahmsen, L., Clemons, N.J., Nordlund, P., Rudd, S.G., Wiman, K.G., 2021. Mutant p53-reactivating compound APR-246 synergizes with asparaginase in inducing growth suppression in acute lymphoblastic leukemia cells. *Cell Death Dis*. 12, 709. https://doi.org/10.1038/s41419-021-03988-y.

[48] Rasheduzzaman, M., Park, S.Y., 2018. Antihypertensive drug-candesartan attenuates TRAIL resistance in human lung cancer via AMPK-mediated inhibition of

autophagy flux. *Exp. Cell Res*. 368, 126–135. https://doi.org/10.1016/j.yexcr.2018.04.022.

[49] Thiery, J.P., Acloque, H., Huang, R.Y.J., Nieto, M.A., 2009. Epithelial-mesenchymal transitions in development and disease. *Cell*. 139, 871–890. https://doi.org/10.1016/j.cell.2009.11.007.

[50] Zhang, J., Fan, J., Venneti, S., Cross, J.R., Takagi, T., Bhinder, B., Djaballah, H., Kanai, M., Cheng, E.H., Judkins, A.R., Pawel, B., Baggs, J., Cherry, S., Rabinowitz, J.D., Thompson, C.B., 2014. Asparagine plays a critical role in regulating cellular adaptation to glutamine depletion. *Mol. Cell*. 56, 205–218. https://doi.org/10.1016/j.molcel.2014.08.018.

[51] Bensaad, K., Cheung, E.C., Vousden, K.H., 2009. Modulation of intracellular ROS levels by TIGAR controls autophagy. *EMBO J*. 28, 3015–3026. https://doi.org/10.1038/emboj.2009.242.

[52] Kim, Y.H., Baek, S.H., Kim, E.K., Ha, J.M., Jin, S.Y., Lee, H.S., Ha, H.K., Song, S.H., Kim, S.J., Shin, H.K., Yong, J., Kim, D., Kim, C.D., Bae, S.S., 2016. Uncoordinated 51-like kinase 2 signaling pathway regulates epithelial-mesenchymal transition in A549 lung cancer cells. *FEBS Lett*. 590, 1365–1374. https://doi.org/10.1002/1873-3468.12172.

[53] Kiyono, K., Suzuki, H.I., Matsuyama, H., Morishita, Y., Komuro, A., Kano, M.R., Sugimoto, K., Miyazono, K., 2009. Autophagy is activated by TGF-beta and potentiates TGF-beta-mediated growth inhibition in human hepatocellular carcinoma cells. *Cancer Res*. 69, 8844–8852. https://doi.org/10.1158/0008-5472.CAN-08-4401.

[54] Li, J., Yang, B., Zhou, Q., Wu, Y., Shang, D., Guo, Y., Song, Z., Zheng, Q., Xiong, J., 2013. Autophagy promotes hepatocellular carcinoma cell invasion through activation of epithelial-mesenchymal transition. *Carcinogenesis*. 34, 1343–1351. https://doi.org/10.1093/carcin/bgt063.